Supporting Information

Rational Mechanochemical Design of Diels–Alder Crosslinked Biocompatible Hydrogels with Enhanced Properties

Sophia J. Bailey,[a] Christopher W. Barney,[b,c] Nairiti J. Sinha,[c,d] Sai Venkatesh Pangali,[e] Craig J. Hawker,[a,c,f] Matthew E. Helgeson,[c] Megan T. Valentine,[b] Javier Read de Alaniz[a]

[a.]Department of Chemistry and Biochemistry, University of California Santa Barbara, Santa Barbara, CA 93106.
[b.]Department of Mechanical Engineering, University of California Santa Barbara, Santa Barbara, CA 93106.
[c.]Department of Chemical Engineering, University of California Santa Barbara, Santa Barbara, CA 93106.
[d.]Materials Research Laboratory, University of California Santa Barbara, Santa Barbara, CA 93106.
[e.]Center for Structural Molecular Biology, Neutron Scattering Division, Oak Ridge National Laboratory, Oak Ridge, TN, 37831
[f.]Materials Department, University of California Santa Barbara, Santa Barbara, CA 93106.

Table of Contents

1. Synthesis of Network Building Blocks

1.1 Materials and Methods

Unless otherwise noted, all chemicals were obtained from Sigma Aldrich, Fisher Scientific or Oakwood Chemical and used as received without further purification and all reactions were performed under an atmosphere of nitrogen. Acetonitrile, tetrahydrofuran, dichloromethane and toluene were dispensed from a solvent purification system immediately before use or stored over 3Å molecular sieves. Ethanol and methanol were also stored over 3Å molecular sieves before use. Thin-layer chromatography (TLC) was conducted with E. Merck silica gel 60 F254 pre-coated plates (0.25 mm) and visualized by exposure to UV light (254 nm) or stained with *p*-anisaldehyde. Flash column chromatography was performed using normal phase silica gel (60 Å, 0.040 – 0.063 mm, Geduran) with hexanes, ethyl acetate (EtOAc), DCM and/or MeOH as eluents. ^{1}H and ^{13}C NMR spectra were recorded on Varian spectrometers (100, 400 or 600 MHz) and are reported relative to $CDCl_3$ (δ = 7.26 ppm for ^{1}H and 77.00 ppm for ^{13}C). Data for ^{1}H NMR spectra are reported as follows: chemical shift (δ ppm), multiplicity, coupling constant (Hz) and integration. Data for ^{13}C NMR spectra are reported in terms of chemical shift (δ ppm). Mass spectra were obtained from the UC Irvine Mass Spectrometry Facility on a time-of-flight mass spectrometer with an ESI source. Size exclusion chromatography (SEC) eluting with chloroform ($CHCl_3$) and calibrated relative to poly(ethylene glycol) standards was performed on a Waters Alliance HPLC System, 2695 separation module equipped with a Waters 2410 differential refractometer and Waters 2998 photodiode array detector.

1.2 Synthesis of Small Molecules

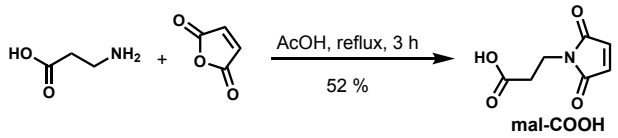

mal-COOH

3-maleimidopropionic acid (mal-COOH):

3-maleimidopropionic acid is *commercially available* (CAS 7423-55-4), but was prepared according to a literature procedure.[1] In a 100 mL round bottom flask, maleic anhydride (6.00 g, 61.2 mmol, 1 eq) and beta-alanine (5.50 g, 61.7 mmol, 1.01 eq) were dissolved in acetic acid (45 mL) and the solution was brought to reflux. After 3 h the solution was cooled to room temperature and the acetic acid was removed under reduced pressure. The residue was subjected to flash column chromatography (2.5% methanol in dichloromethane) to afford **mal-COOH** (5.38 g, 31.8 mmol, 52 %) as a white powder. Spectral data matches reported literature.[1]

^{1}H NMR (400 MHz, $CDCl_3$) δ 10.87 (brs, 1H), 6.72 (s, 2H), 3.84 (t, *J* = 7.2 Hz, 2H), 2.71 (t, *J* = 7.2 Hz, 2H) ppm.

The compound was further purified by recrystallization from hot water to afford colorless crystals before being used to functionalize **tetraPEG**.

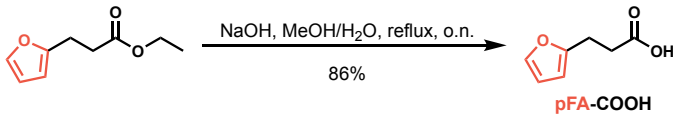

2-furanpropionic acid (pFA-COOH):
2-furanpropionic acid is *commercially available* (CAS 935-13-7) but was prepared from the more affordable ester precursor (CAS 10031-90-0). In a 500 mL round bottom flask ethyl 3-(furan-2-yl)propionate (7.20 g, 42.8 mmol, 1 eq) was dissolved in in methanol (MeOH, 75 mL) before 2.5 M NaOH (200 mL) was slowly added. The solution was refluxed overnight (15.5 h) before cooling to rt. The solution was neutralized with 3 M HCl and extracted with dichloromethane (3 X 200 mL). The combined organic layers were washed with brine (100 mL), dried over magnesium sulfate, and concentrated under reduced pressure to afford **pFA-COOH** (5.13 g, 36.6 mmol, 86 %) as an off-white solid. Spectral data matches reported literature.[2]

^{1}H NMR (600 MHz, $CDCl_3$) δ 10.67 (brs, 1H), 7.32 – 7.30 (m, 1H), 6.29 – 6.27 (m, 1H), 6.05 – 6.04 (m, 1H), 2.98 (t, *J* = 7.5 Hz, 2H), 2.72 (t, *J* = 7.6 Hz, 2H) ppm.

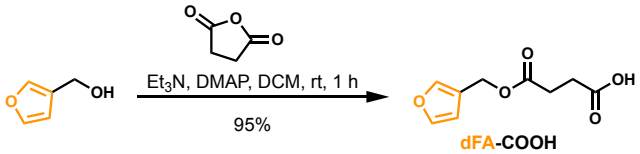

4-(furan-3-ylmethoxy)-4-oxobutanoic acid (dFA-COOH):
In a scintillation vial equipped with stir bar furan-3-methanol (CAS 4412-91-3) (1.72 mL, 20.0 mmol, 1 eq) was dissolved in dichloromethane (DCM) (7.5 mL), then triethyl amine (2.79 mL, 20.0 mmol, 1 eq), 4-dimethylaminopyridine (DMAP, 244 mg, 2.00 mmol, 0.1 eq), and succinic anhydride (2.60 g, 26.0 mmol, 1.3 eq) were added. The reaction was stirred at rt until complete consumption of the starting material (TLC, 1 h). The solution was transferred to a separatory funnel along with additional DCM (50 mL). The organic layer was washed with 1 M HCl (2 X 50 mL) then water (1 X 50 mL) and dried over magnesium sulfate. The solvent removed to afford **dFA-COOH** (3.76 g, 19.0 mmol, 95%) as an off-white solid.

dFA-COOH: ^{1}H NMR (600 MHz, $CDCl_3$) δ 7.47 (m, 1H), 7.40 (m, 1H), 6.42 (m, 1H), 5.02 (s, 2H), 2.71 – 2.64 (m, 4H) ppm; ^{13}C NMR (125 MHz, $CDCl_3$) δ 177.56, 171.99, 143.44, 141.61, 120.14, 110.49, 58.11, 28.82, 28.77 ppm; HRMS (ES+) Exact mass cald. for $C_9H_{10}O_5Na$ $[M+Na]^+$: 221.0426, found: 221.0426.

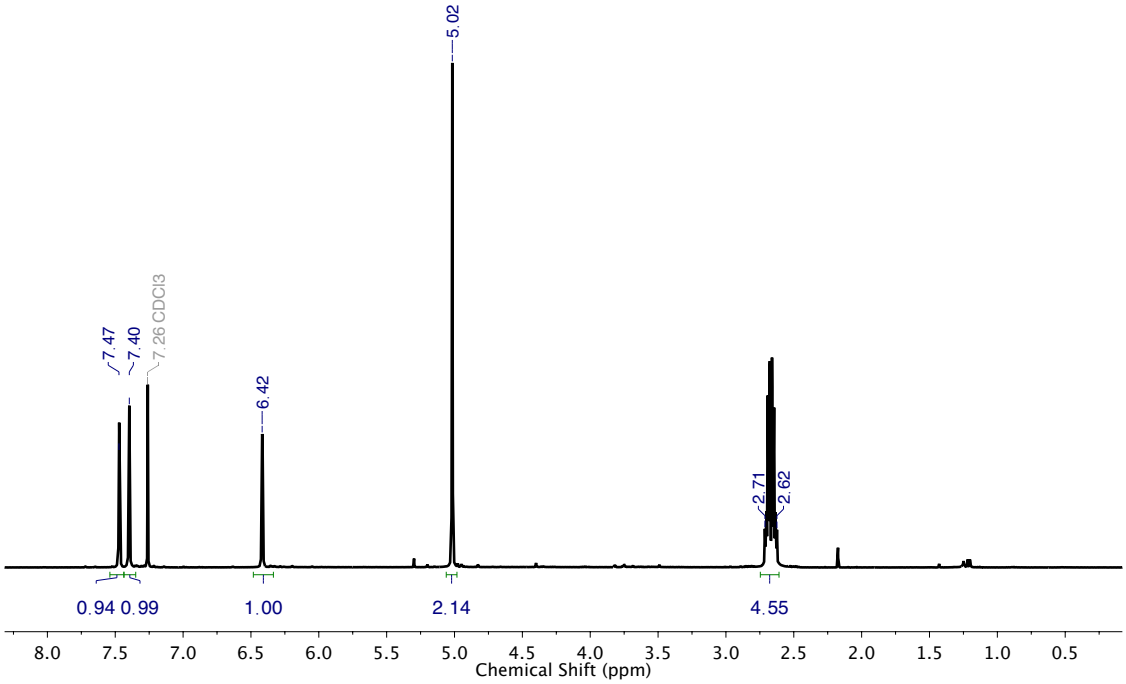

Figure S1. ^{1}H NMR (400 MHz, $CDCl_3$) **dFA-COOH**

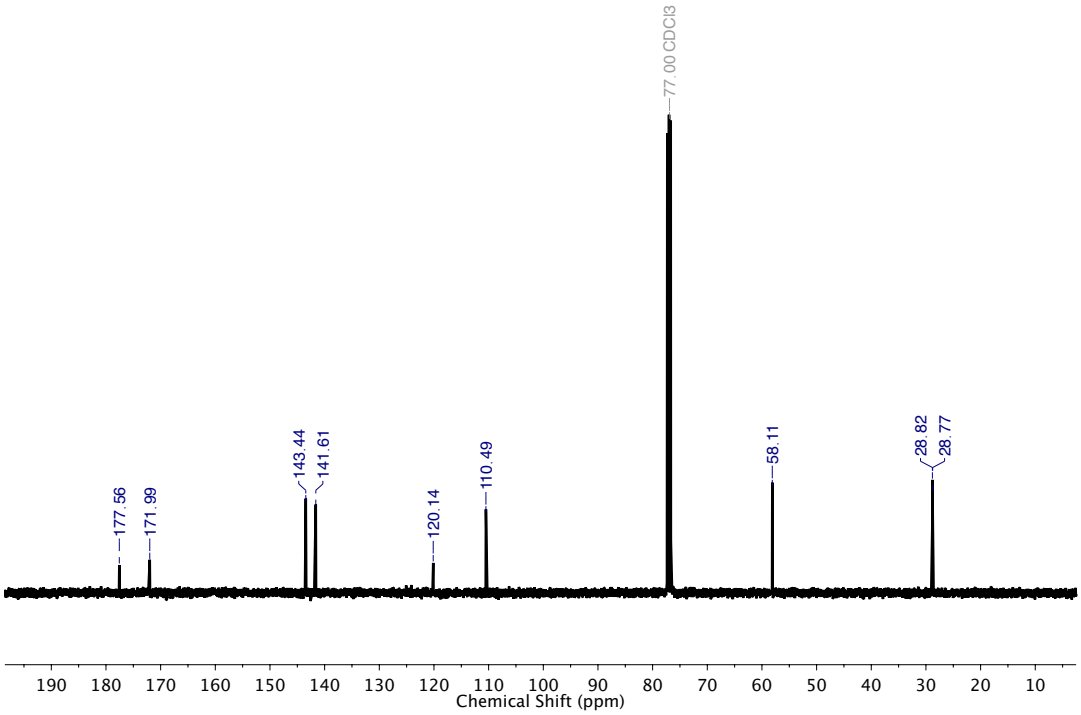

Figure S2.^{13}C NMR (125 MHz, $CDCl_3$) **dFA-COOH**

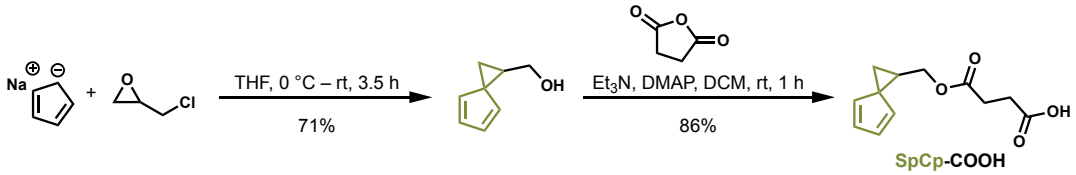

(SpCp-COOH):

SpCp-COOH was prepared according to a literature procedure.[3]

Step 1: Epichlorohydrin (4.05 mL, 51.7 mmol, 1 eq) was dissolved in tetrahydrofuran (200 mL) in a flame dried, 1 L round bottom flask equipped with dropping funnel. The solution was cooled to 0 °C before sodium cyclopentadienylide (100 mL, 2-3 M solution purchased from Strem Chemical) was added dropwise and allowed to stir for 3.5 h (at which point complete consumption of epichlorohydrin was confirmed by ^{1}H NMR). To the solution was added H_2O (200 mL) followed by saturated sodium bicarbonate (200 mL) before extracting with diethyl ether (3 X 200 mL). The combined organic layers were washed with brine (200 mL), dried over magnesium sulfate, and concentrated under reduced pressure. The residue was subjected to flash column chromatography (hexanes:ethyl acetate, 2:1) to afford **SpCp-OH** (4.36 g, 35.7 mmol, 71 %).

Step 2: In a scintillation vial equipped with stir bar **SpCp-OH** (1.28 g, 10.4 mmol, 1 eq) was dissolved in DCM (3 mL), then triethyl amine (1.45 mL, 10.4 mmol, 1 eq), DMAP (127 mg, 1.04 mmol, 0.1 eq), and succinic anhydride (1.36 g, 13.6 mmol, 1.3 eq) were added. The reaction was stirred at rt until complete consumption of the starting material (TLC, 1 h). The solution was transferred to a separatory funnel along with additional DCM (100 mL). The organic layer was washed with 1 M HCl (2 X 75 mL) then water (1 X 75 mL) and dried over magnesium sulfate. The solvent removed to afford **SpCp-COOH** (1.99 g, 8.95 mmol, 86 %) as a yellow-white solid. Spectral data matches reported literature.[3]

^{1}H NMR (400 MHz, $CDCl_3$) δ 9.85 (brs, 1H) 6.57 (dt, *J* = 5.2, 1.9 Hz, 1H), 6.48 (dt, *J* = 5.1, 1.5 Hz, 1H), 6.20 (dt, *J* = 5.2, 1.7 Hz, 1H), 6.06 (dt, *J* = 5.1, 1.7 Hz, 1H), 4.35 (dd, *J* = 11.7, 7.5 Hz, 1H), 4.18 (dd, *J* = 11.6, 7.3 Hz, 1H), 2.69 – 2.60 (m, 4H), 2.41 (quin, *J* = 7.3 Hz, 1H), 1.83 (dd, *J* = 8.6, 4.5 Hz, 1H), 1.67 (dd, *J* = 7.0, 4.5 Hz, 1H) ppm.

1.3 Chain-end Functionalization of Poly(ethylene glycol)

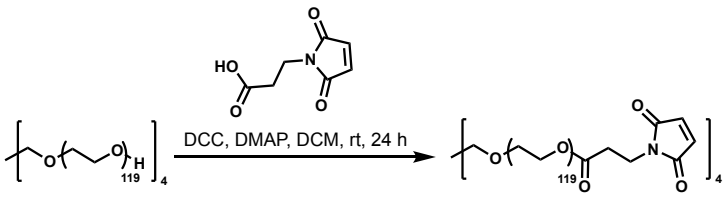

Poly(ethylene glycol)-tetra-maleimide:

In a 200 mL round bottom flask equipped with stir bar **tetraPEG** (purchased from JenKem Technology, M_n = 20,000 g/mol, 40.0 g, 2.00 mmol, 1 eq) was dissolved in dichloromethane 80 mL. To this solution was added **mal-COOH** (3.38 g, 20.0 mmol, 10 eq), *N,N'*-Dicyclohexylcarbodiimide (DCC, 4.54 g, 22.0 mmol, 11 eq), and 4-dimethylaminopyridine (DMAP, 24.4 mg, 0.200 mmol, 0.1 eq). The solution was allowed to stir at rt for 24 h (at which point complete formation of the ester was confirmed by ^{1}H NMR). The reaction solution then was passed through a plug of celite before the solvent was removed under reduced pressure. The residue was taken up in ethanol (EtOH, 800 mL), cooled to 0 °C and left unagitated for 30 minutes to allow **tetramalPEG** to precipitate. The solid was filtered and rinsed with cold EtOH then diethyl ether. The precipitate was thoroughly dried under reduced pressure to afford **tetramalPEG** (27.7 g, 1.32 mmol, 66% recovered yield) as a pink-white solid. $M_{n(NMR)}$ (DP = 119/arm) = 21,500 g/mol, $M_{n(SEC)}$ = 17,000 g/mol, $Đ$ = 1.14.

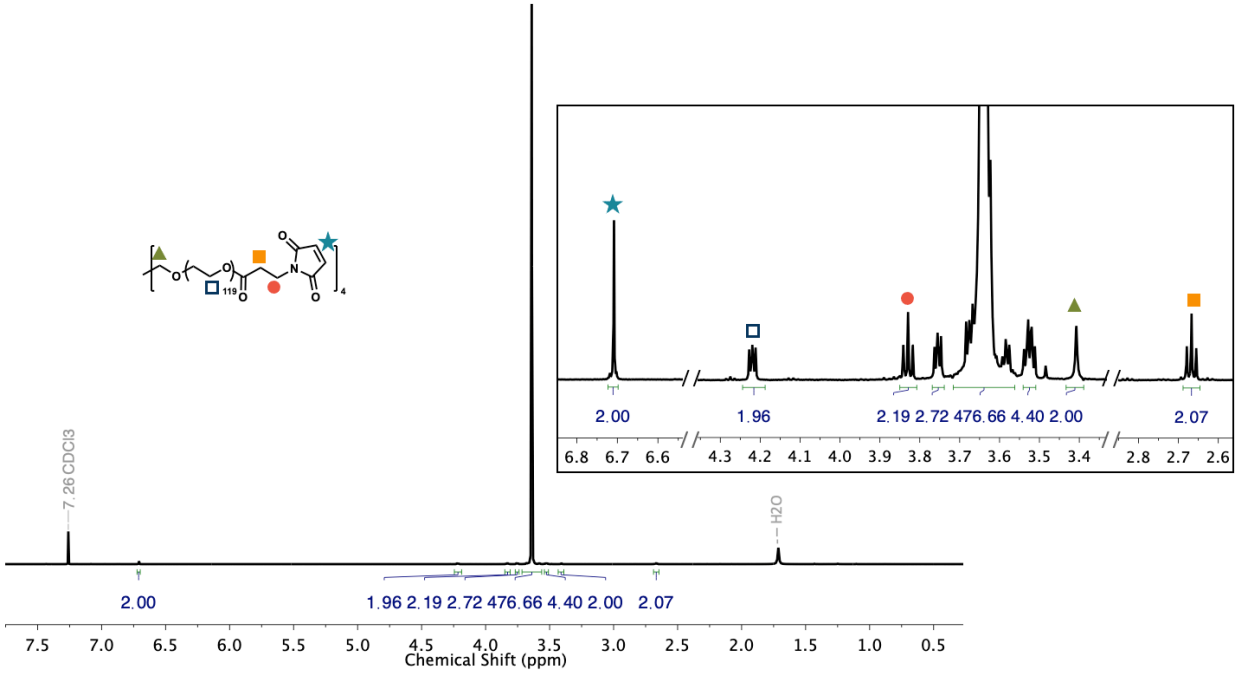

Figure S3. ^{1}H NMR (600 MHz, $CDCl_3$) **tetramalPEG** indicates quantitative chain-end functionalization with maleimide.

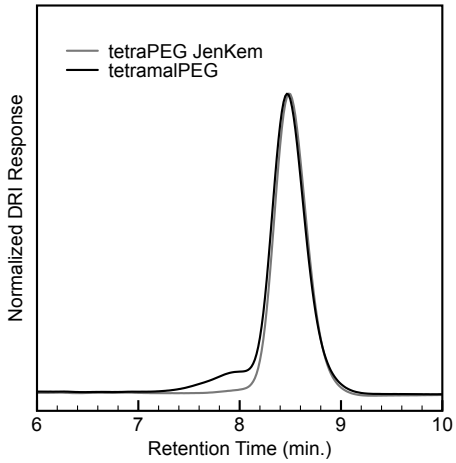

Figure S4. Overlay of size exclusion chromatography (SEC) trace of starting tetraPEG and product **tetramalPEG**

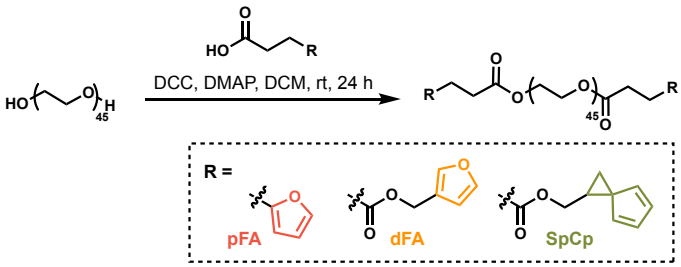

General Procedure for bisdiene-PEG functionalization:

Poly(ethylene glycol) (purchased from Sigma Aldrich, M_n = 2,000 g/mol, 1 eq) was dissolved in DCM to afford a 0.125 M solution of polymer. To this solution was then added the diene carboxylic acid (SpCp-COOH, pFA-COOH or

dFA-COOH, 4 eq), DCC) (3 eq), and DMAP (0.2 eq). The solution was allowed to stir at rt for 24 h (at which complete formation of the ester was confirmed by crude ^{1}H NMR). The reaction solution then was passed through a plug of celite before the solvent was removed under reduced pressure. The residue was taken up in ethanol (EtOH, 100 mL/g PEG), cooled to 0 °C and left unagitated for 30 minutes to allow the polymer to precipitate. The solid was filtered and rinsed with cold EtOH then diethyl ether before being thoroughly dried under reduced pressure to afford the diene functionalized polymers as waxy solids.

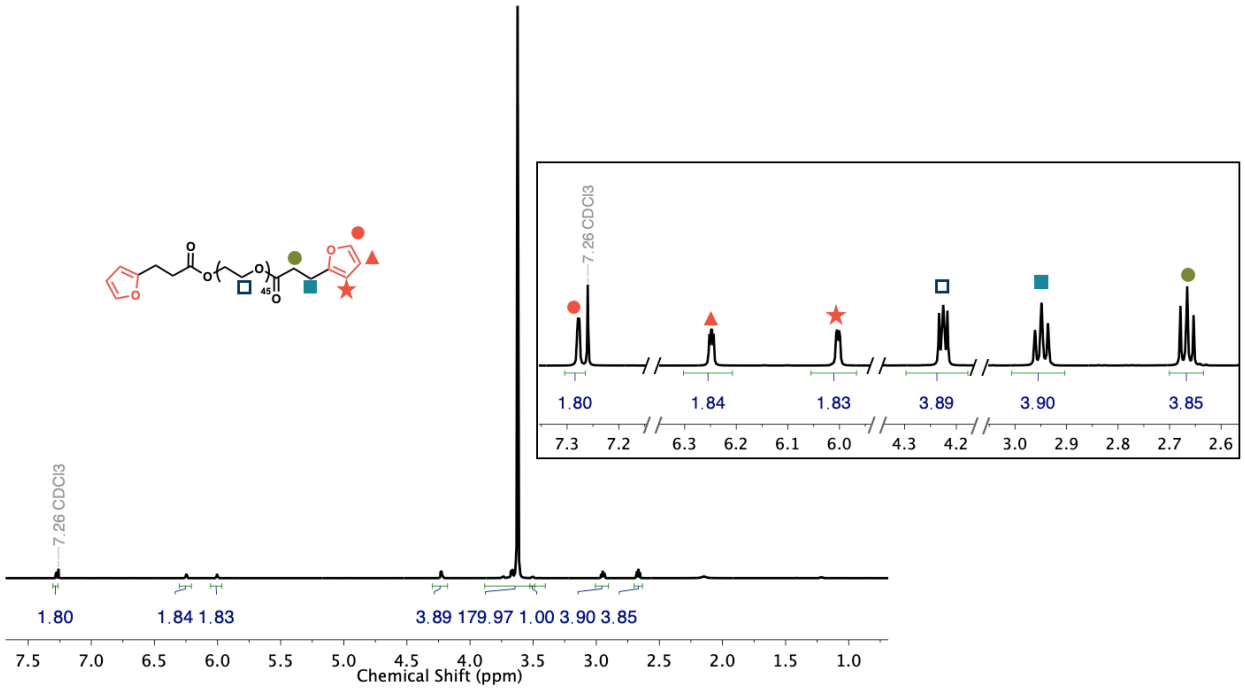

Figure S5. ^{1}H NMR (600 MHz, $CDCl_3$) **bispFAPEG** ($M_{n(NMR)}$ = 2,300 g/mol) indicates quantitative chain-end functionalization with *proximal* furan (pFA).

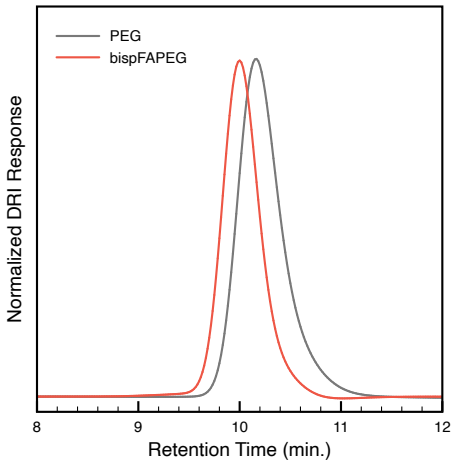

Figure S6. Overlay of SEC trace of starting PEG and product **bispFAPEG**, $M_{n(SEC)}$ = 3,100 g/mol, $Đ$ = 1.05.

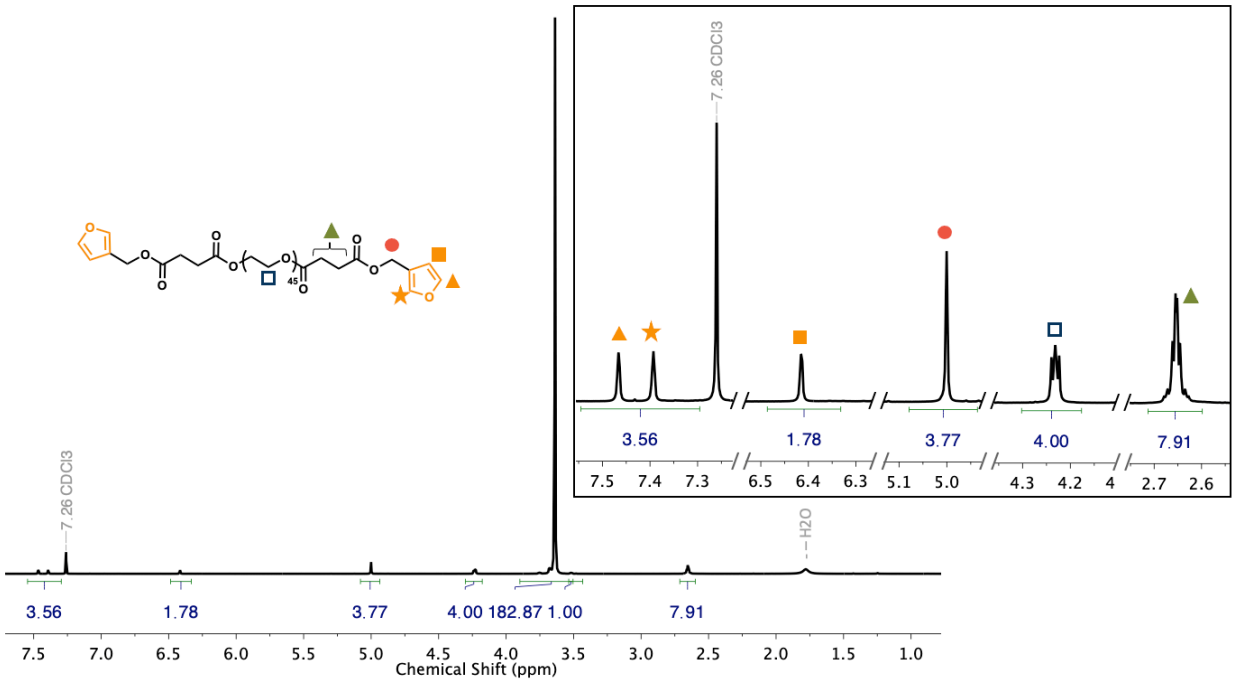

Figure S7. ^{1}H NMR (600 MHz, $CDCl_3$) **bisdFAPEG** ($M_{n(NMR)}$ = 2,400 g/mol) indicates quantitative chain-end functionalization with *distal* furan (dFA).

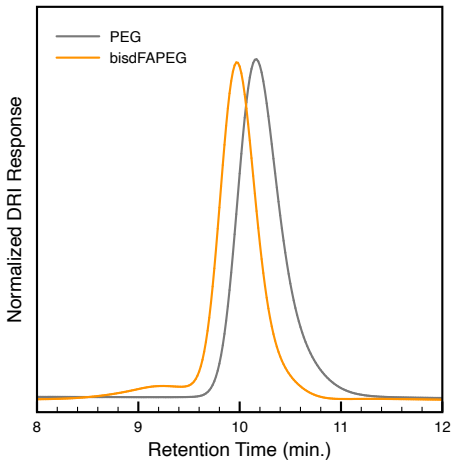

Figure S8. Overlay of SEC trace of starting PEG and product **bisdFAPEG**, $M_{n(SEC)}$ = 3,300 g/mol, $Đ$ = 1.09.

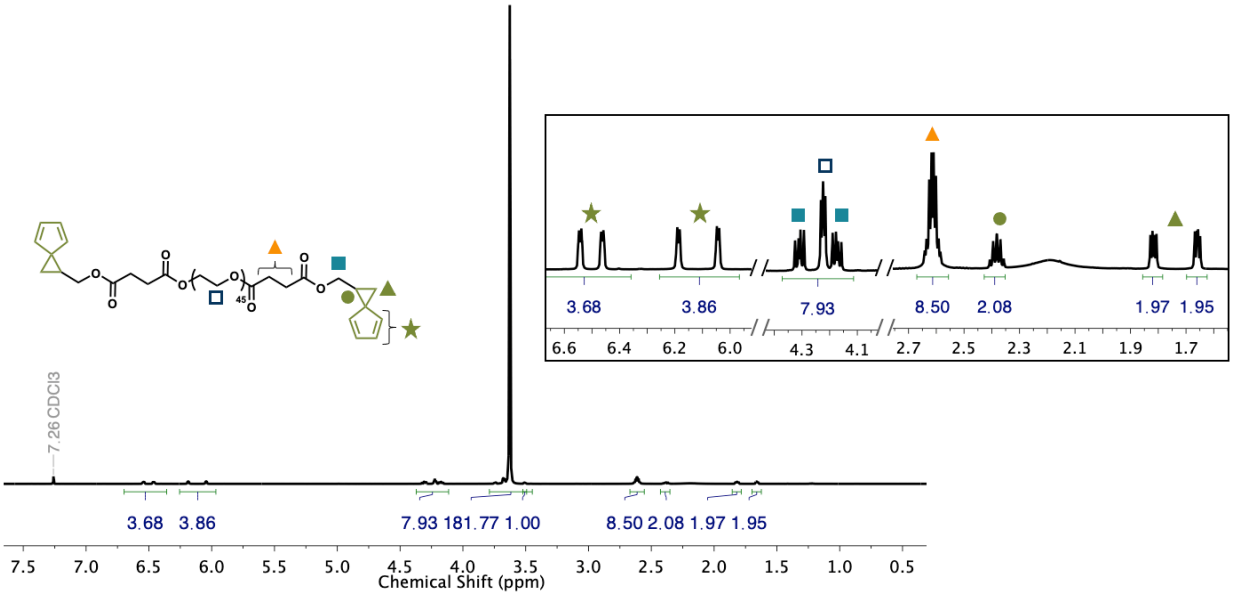

Figure S9. ^{1}H NMR (600 MHz, $CDCl_3$) **bisSpCpPEG (**$M_{n(NMR)}$ = 2,400 g/mol) indicates quantitative chain-end functionalization with spiro[2.4]hepta-4,6-diene (SpCp).

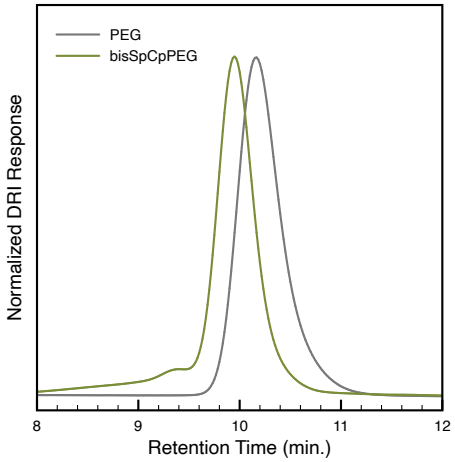

Figure S10. Overlay of SEC-RI trace of starting PEG and product **bisdFAPEG**, $M_{n(SEC)}$ = 3,400 g/mol, $Đ$ = 1.15.

1.4 Hydrogel Preparation

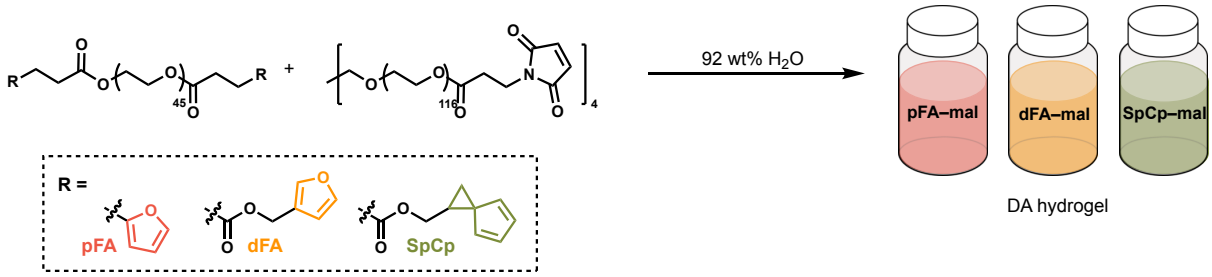

General Procedure for Hydrogel Preparation:
To prepare multiple samples (15 – 17 mL/sample) for indentation and puncture experiments, large batches of pre-hydrogel solutions were prepared and transferred into scintillation vials, capped, and sealed with parafilm for 10 days before puncture experiments. To prepare pre-hydrogel solutions, **tetramalPEG** and each **bisdiene PEG** were dissolved at 8 wt% polymer in deionized water. The solutions were then combined to achieve stoichiometric balance between maleimide, and diene chain ends as indicated in Table S1.

Table S1. Hydrogel formulations

Linker Type	mmol tetramalPEG	mass 8 wt% solution tetramalPEG (g)	MW bisdiene PEG (g/mol)	mmol bisdienePEG	mass 8wt% solution tetramalPEG (g)
pFA	0.214	**56.25**	2300	0.428	**12.32**
dFA	0.214	**56.25**	2400	0.428	**12.86**
SpCp	0.214	**56.25**	2400	0.428	**12.86**

For SpCp, gelling is rapid (<2 min), thus upon combining the two solutions, care was taken to avoid the introduction of bubbles while mixing solutions, then the viscous pre-hydrogel was quickly distributed between scintillation vials. For pFA and dFA, gelling was much slower and solution preparation was completed without issue.

1.5 Gel Fraction and Swelling Ratios

For determination of gel fraction and swelling ratio, small hydrogels (approx. 100 mg polymer) were prepared in dram vials from the solutions described in Section 1.4. After 10 days the gels were removed from the vials and dried under reduced pressure for 24 h to measure the initial sol + gel mass (W_i). Each gel was then allowed to swell in 150 mL of water for 36 h (exchanging the solvent once) before the equilibrium swelling mass (W_s) was measured. The gels were again dried under reduced pressure for 24 h to afford dry gel mass (W_d). Each hydrogel type was prepared and investigated in triplicate and results of these studies are summarized in Table S2.

$$\text{gel fraction} = \frac{Wd}{Wi} \times 100$$

$$Q = \frac{Ws - Wd}{Wd}$$

Table S2. Summary of gel fraction and swelling behavior for each hydrogel.

Hydrogel Type	Gel Fraction	Eq. Swelling Ratio, Q
pFA	96 ± 4 %	18 ± 4
dFA	98 ± 3%	17 ± 2
SpCp	94 ± 4%	18.6 ± 0.2

2. Indentation and Puncture Measurements

Indentation measurements were used to monitor the curing process while puncture measurements were used to quantify the failure strength. Both measurements were performed on a TA.XT Plus Connect Texture Analyzer. The instrument has a load cell with a force capacity of 49 N and a displacement resolution of 1 µm. Indentation was performed with a 2 mm diameter flat steel cylinder moving at a displacement rate of 0.1 mm/s to a max turnaround force of 20 mN. The observed stiffness κ can be used in conjunction with the contact radius a and sample height h ($\approx 30\ mm$) to extract Young's modulus E (Equation 1).[4]

$$E = \frac{3}{8a}\kappa\left[1 + 1.33\frac{a}{h} + 1.33\left(\frac{a}{h}\right)^3\right]^{-1} \qquad \text{(Equation 1)}$$

Migration of solvent is known to cause shifts in observed the stiffness for gels.[5] This poroelastic effect is typically quantified by comparing the poroelastic relaxation time $\tau_{poro} = \frac{a^2}{D}$, where D is the diffusion coefficient of solvent in the network, to the time scale of the test. Estimating $D = 4.4 \times 10^{-10}\ m^2/s$, measured from the diffusion of water through a PEG methacrylate gel,[6] gives a value of $\tau_{poro} \approx 2200\ s$ which is much longer than the test time of approximately 60 s. Due to this difference in time scales, it is not likely that poroelastic relaxation is significantly altering the stiffness observed with this measurement. E values for each gel were monitored over several days to let the gels cure to completion. A summary of this data is available in Table S3.

Table S3. Table showing the curing data collected at different times.

Cure Time (Days)	pFA E (kPa)	Cure Time (Days)	dFA E (kPa)	Cure Time (Days)	SpCp E (kPa)
4	8.3±0.6	1.85	0.101±0.004	0.02083	14.83±0.05
8	9.7±0.2	3.725	3.63±0.01	1.89583	15.5±0.2
10	9.9±0.1	6.6833	8.72±0.02	4.8542	15.3±0.1
23	10.1±0.1	8.6208	10.66±0.02	6.7917	15.1±0.1
38	10.3±0.1	10.85	11.83±0.05	9.0209	15.0±0.1
		14.642	12.18±0.06	12.8126	14.6±0.1
		16.767	11.85±0.02	14.9376	14.5±0.2

Puncture measurements were used to quantify the failure strength of the gels once curing had occurred. Puncture measurements were performed with a 22 gauge (207 μm inner radius and 359 μm outer radius) blunt-tipped steel needle sourced from Hamilton Company. A similar calculation to that performed for indentation above gives $\tau_{poro} \approx 293\ s$ while the testing time is kept at approximately 60 s by increasing the displacement rate to 1 mm/s. Puncture tests are performed by inserting a needle into a gel at a constant displacement rate to a displacement beyond the puncture point.[7] An example plot of the force displacement curve observed during puncture of a gel with dFA linkers is shown in Figure S11a. The initial elastic loading curve is nonlinear in nature and has been shown to be well modeled with an empirically derived force-displacement relationship,[7]

$$F = k'Ed^2 + k''ERd, \qquad \text{(Equation 2)}$$

where F is force, d is displacement, R is indenter radius, and both k' and k'' are fitting constants that appear to be characteristic for different materials.[7–10] The elastic loading phase terminates in puncture of the gel. Puncture of the gel displays a characteristic drop in the force-displacement curve giving a critical puncture force F_c and displacement d_c. Here displacement is normalized to the initial contact point between the needle and the gel surface. This point is defined by convention here as occurring once the measured force value reaches 10 mN which is well above the 1 mN noise threshold of the load cell. This results in a small yet consistent underestimation error

in the values reported here for d_c. Assuming Hertzian contact holds in this low strain regime then the samples with pFA, dFA, and SpCp linkers are expected to overestimate the initial contact displacement by 1.0, 0.9, and 0.7 mm, respectively, which translates to an approximate underestimation of d_c by 7.4%, 4.6%, and 3.5% respectively.

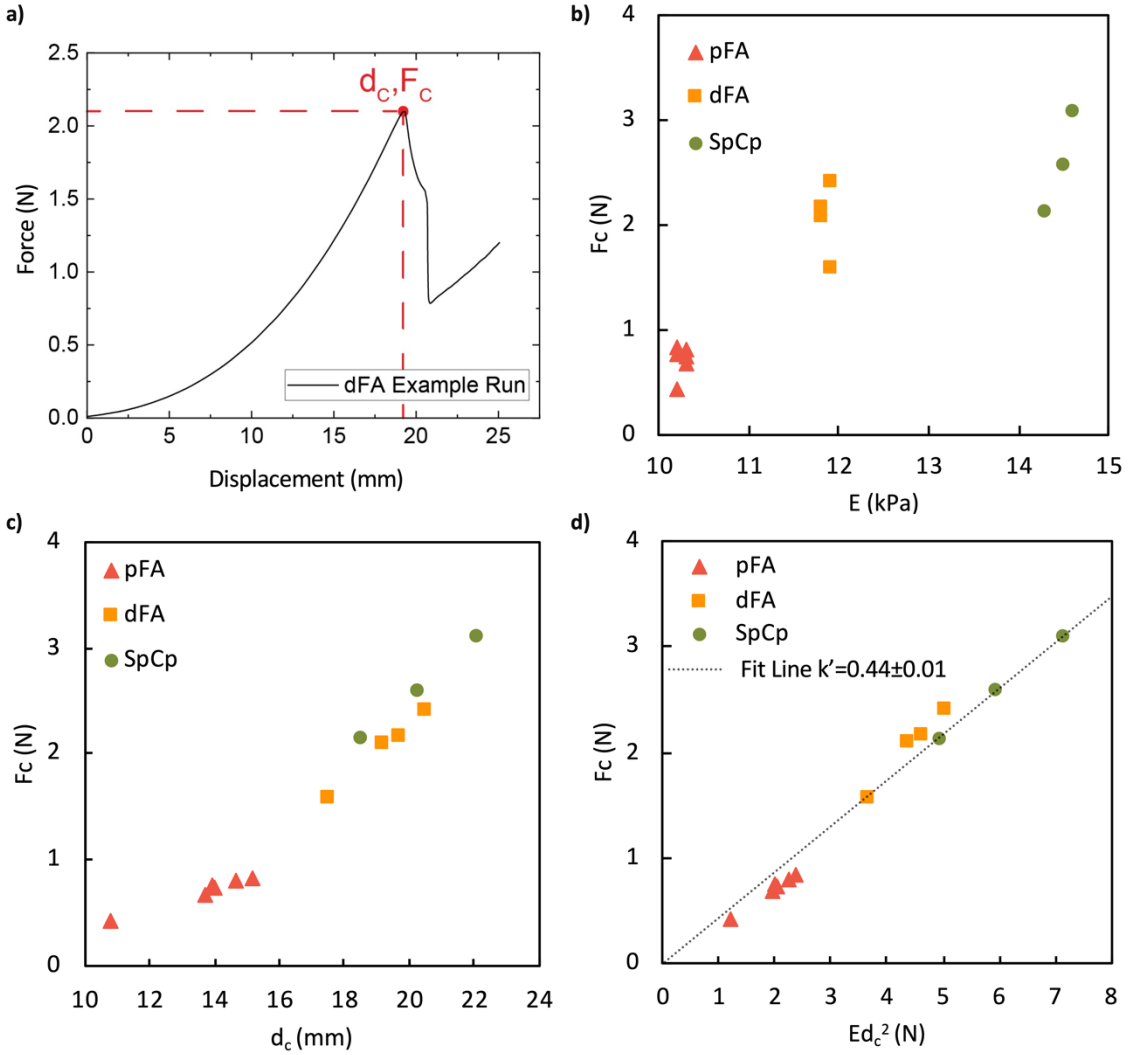

Figure S11. a) A plot showing an example force-displacement curve for a dFA sample. b-c) Plots of F_c against E and d_c showing that F_c is a function of both variables. d) Plot of F_c against $Ed_c{}^2$ where the observed linear collapse justifies the treatment of k' as a constant value.

A comparison of F_c against E is shown in Figure S11b. This comparison shows there is a systematic increase in F_c as E increases between the samples. A similar comparison between F_c and d_c in Figure S11c shows that there is also a systematic increase in F_c as d_c increases. The systematic variation of F_c with both E and d_c is of concern as this suggests that the changes observed in F_c may be conflated by changes in E. From the molecular perspective, it is true that both modulus and fracture toughness have an explicit dependence on the crosslinking density. According to Lake-Thomas theory,[11] $G_c \sim \sqrt{N}$ where G_c is the fracture toughness and N represents the number of Kuhn segments between crosslinks. According to statistical theory,[12] $E \sim N^{-1}$ where E is Young's modulus giving that $G_c \sim E^{-1/2}$ when altering the number of elastically effective crosslinks at constant network concentration. If the weakest bond strengths in our networks were equal, this would predict that G_c should increase by a factor of approximately 1.22 when going from SpCp samples to pFA samples. If this translated directly to a change in F_c (past measurements[10] have observed that $\frac{F_c}{R} \sim \sqrt{G_c}$ which would predict an increase of 10%), this would predict a 22% increase in the puncture force of the pFA samples relative to the SpCp samples instead of the 72% decrease

observed experimentally. This decrease is most likely associated with the fact that we are altering the weakest bond in our system and $G_c \sim U$ where U is related to the strength of the weakest bond in the system. Our results here suggest that the crosslinking density is not altered enough to overcome the changes induced by weakening the bonds in the system and that these changes are better quantified using our understanding of the mechanics at the continuum level.

The impact of E and d_c on F_c can be estimated by substituting into Equation 2 and ignoring the lower order term ($k'' = 0$) to get Equation 3.

$$F_c = k' E {d_c}^2 \qquad \text{(Equation 3)}$$

The plot of F_c against $E{d_c}^2$ in Figure S11d confirms that k' is reasonably well approximated with a constant value of 0.44 ± 0.01 for the gels used in this study. This agreement suggests that this relationship is valid for these gels and can be used to deconvolute the impact that changes in E and d_c have on F_c. Taking the pFA samples as a reference point, the values of F_c predicted from the observed changes in E and d_c are shown in Figure S12. These calculations are performed by taking the changes in E and d_c in combination with the above equation to estimate the change in F_c relative to the pFA samples used here as a reference point. This can be expressed as follows:

$$F_{c,pred} = F_{c,ref}\left(\frac{E_{obs}}{E_{ref}}\right)\left(\frac{d^2_{c,obs}}{d^2_{c,ref}}\right) \qquad \text{(Equation 4)}$$

where $F_{c,pred}$ is the predicted value of the critical puncture force, E_{obs} and $d_{c,obs}$ are the observed values of the Young's modulus and critical puncture displacement, respectively, and $F_{c,ref}$, E_{ref} and $d_{c,ref}$ refer to reference values of the same. For example, the average values of E and d_c for the pFA and dFA samples are 10.3 kPa and 11.85 kPa, respectively, and 13.73 mm and 19.3 mm, respectively. Using the ratio approach described in Equation 4, we find a predicted multipliers of $\left(\frac{E_{obs}}{E_{ref}}\right)$ =1.15 and $\left(\frac{d^2_{c,obs}}{d^2_{c,ref}}\right)$ =1.98 resulting in a total predicted multiplier of 2.28. However, the linear relationship that we observed between both E and F_c and d_c^2 and F_c suggests that the 15% increase that is expected from the change in E, will influence the 1.98 multiplier value. Assuming a linear relationship between E_c and d_c^2 we estimate the amplitude of this effect to be 0.15*1.98, which gives a value of 0.297 and a total multiplier value of 1.98+0.297=2.277. Normalizing this value by the total predicted multiplier suggests that the predicted shift in F_c that is attributable to changes in E is $\frac{0.297}{2.277} \times 100 = 13.04\%$. Similar calculations comparing SpCp samples to the pFA samples suggest that 29.1% of the observed change in F_c is attributable to changes in E, as summarized in Table S4.

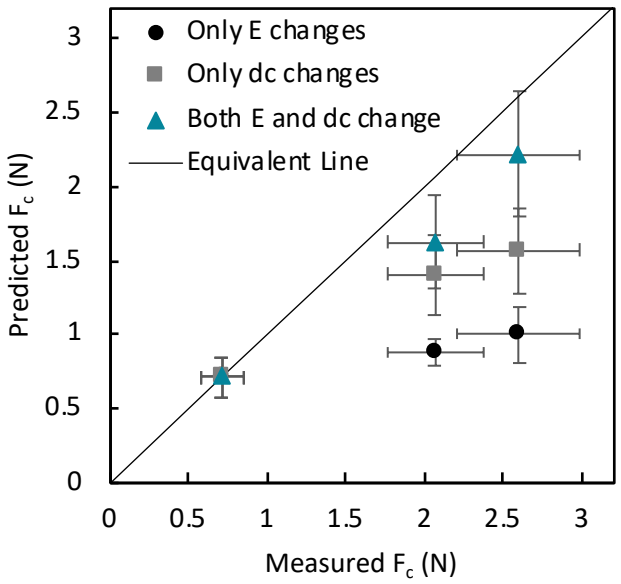

Figure S12. Plot showing predicted changes in F_c due to changes in E and d_c predicted using pFA gels as a reference point in conjunction with Equation 3.

Table S4. Summary of predicted values of F_c plotted in Figure S12.

		Predicted Fc (N)		
Sample	Measured Fc (N)	Only E Changes	Only dc Changes	Both E and dc change
pFA	0.7135±0.1340	Ref. Point	Ref. Point	Ref. Point
dFA	2.0674±0.3025	0.887±0.088	1.41±0.27	1.63±0.31
SpCp	2.6044±0.3914	1.006±0.189	1.57±0.29	2.21±0.42

Puncture of the gel occurs due to the nucleation of a crack near the needle. Past observations have shown that this crack morphology can be quite complex and likely relates to tip geometry, materials properties, and materials defects.[13–15] Two different crack morphologies were observed during the puncture measurements performed for this study. The first is the cone-like crack morphology that has been observed and reported previously.[15] Example images and schematic representations of this morphology at different points during the puncture process are shown in Figure S13 and video of this run is shown in supplementary video SV1. Notably, propagation of a conical crack fails to release strain energy from a large volume of material below the indenter and can both support post-puncture forces that are significantly higher than the puncture force and display a nonlinear force-displacement relationship in the post-puncture regime. The second crack morphology observed during puncture measurements is a combination of those previously reported in the literature. This crack morphology starts as a conical crack and then transitions into a tube-like crack morphology. Example images and schematic representations of this morphology at different points during the puncture process are shown in Figure S14 and video of the run is shown in supplementary video SV2. The transition between crack morphologies appears to be associated with an abrupt deflection of the needle tip in the radial plane. This deflection is associated with the drop in force observed at approximately 26 s in Figure S14. Together these observations suggest that the crack morphology may shift because the bending stiffness of the indenter is low enough to enable the tip to deflect and follow the path of least resistance. A summary of the puncture data gathered in this study, including the crack morphology observed, is contained in Table S5.

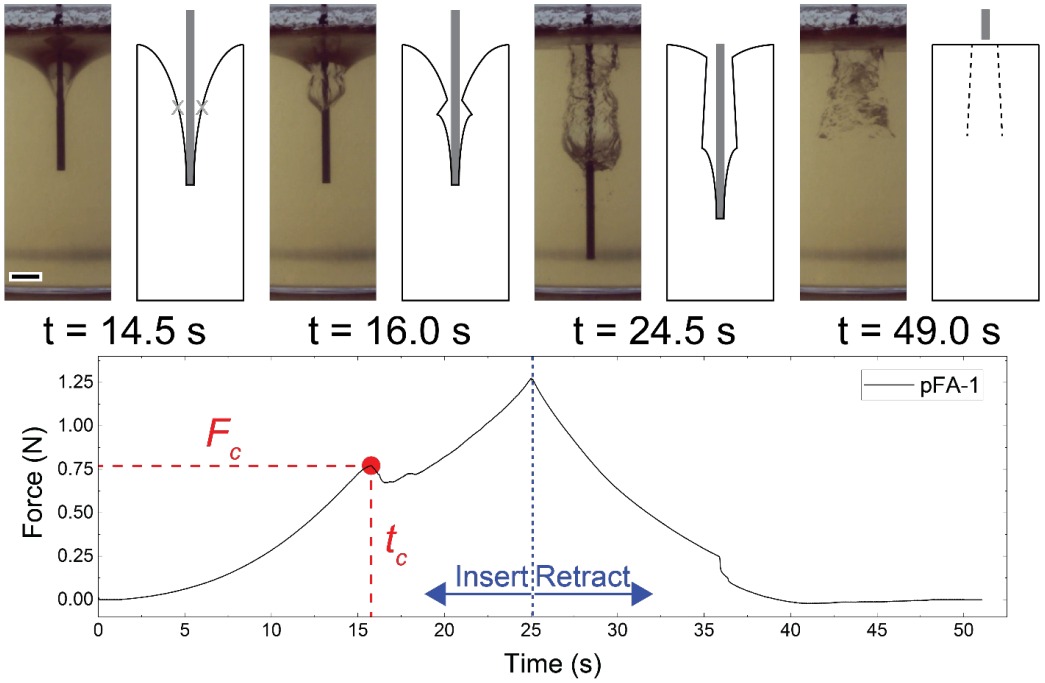

Figure S13. Images and schematic representations of the nucleation and propagation of a conical crack during puncture at different points during the puncture process. From the left, there is deep indentation before puncture, post-puncture, post-propagation near the turnaround point, and the leftover morphology once the needle in fully retracted. The scale bar on the first image represents 2.5 mm.

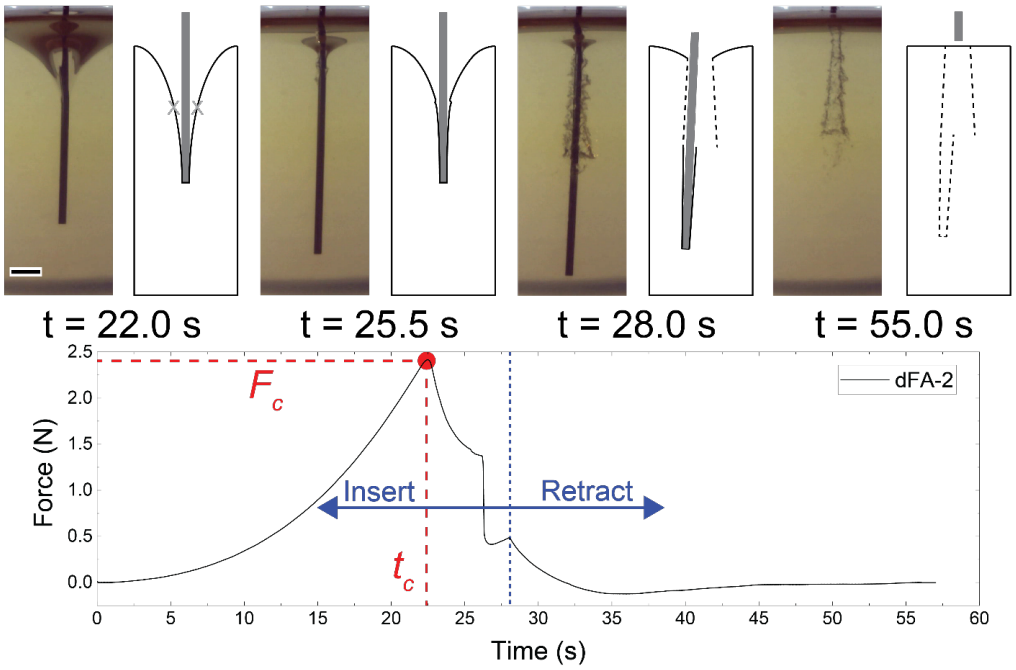

Figure S14. Images and schematic representations of the nucleation and propagation of a cone and tube type crack during puncture at different points during the puncture process. From the left, there is deep indentation before puncture, post-puncture, post-propagation near the turnaround point, and the leftover morphology once the needle in fully retracted. The scale bar on the first image represents 2.5 mm.

Table S5. Summary of the puncture data taken for the samples in this study. Sample denotes the material used for that specific run. Needle radius shows the outer radius of the needle used during puncture. E reports the values of Young's modulus measured via indentation. d_c and F_c stand for the critical puncture displacement and force. Crack morphology reports the type of crack observed during the puncture process. C denotes conical cracks and C+T denotes cone and tube cracks.

Sample	Needle Radius (mm)	E (kPa)	d_c (mm)	F_c (N)	Crack Morphology
pFA-1	0.359	10.2	13.95	0.769	C
pFA-2	0.359	10.3	13.72	0.683	C+T
pFA-3	0.359	10.3	14	0.745	C+T
pFA-4	0.359	10.3	14.67	0.809	C+T
pFA-5	0.359	10.2	10.82	0.435	C+T
pFA-6	0.359	10.2	15.22	0.84	C+T
dFA-1	0.359	11.9	17.529	1.5851	C+T
dFA-2	0.359	11.8	19.19	2.0949	C
dFA-3	0.359	11.9	20.553	2.41557	C+T
dFA-4	0.359	11.8	19.735	2.17404	C+T
SpCp-1	0.359	14.7	--	--	C+T
SpCp-2	0.359	14.6	22.087	3.09405	C+T
SpCp-3	0.359	14.5	20.267	2.58316	C+T
SpCp-4	0.359	14.3	18.546	2.13612	C+T

3. Scattering Measurements

Small-angle neutron scattering measurements were performed using the Bio-SANS instrument located at the High Flux Isotope Reactor in Oak Ridge National Laboratory.[16,17] A single standard configuration of the dual detector system was set with the Panel Scan feature of the instrument with the small-angle detector at 7m and the wide-angle detector at 1.3m and 3.2° to the sample position.[18] Using this configuration, the Q range spanning 0.007 < Q (Å-1) < 1 was obtained using 6 Å wavelength neutrons with a relative wavelength spread (Δλ/λ) of 15%, ($Q = 4\pi \sin(\theta) / \lambda$, with scattering angle as 2θ and wavelength, λ). The data were corrected for instrument background, detector sensitivity, and instrument geometry using facility data reduction software, drt-SANS. All SANS measurements were performed in 1 mm path length glass cell. To prepare samples for scattering, 8 wt% solutions of **tetramalPEG** and each **bisdiene PEG** were prepared by dissolving each polymer in deuterium oxide (D, 99.9% Cambridge Isotope Laboratories) and small-scale pre-hydrogel solutions (100 mg PEG) were prepared in stoichiometric ratio as described in Section 1.4. Once mixed, the pre-hydrogel solutions were quickly transferred into glass cells of dimensions 1 X 20 X 20 mm which were sealed with parafilm and allowed to cure for 10 days at rt before storing at 5 °C until scattering data was obtained. Scattering data for each cell was obtained at 20 °C and scattering signal was recorded in the entire accessible q-range of 0.0009 $Å^{-1}$ to 1 $Å^{-1}$ and the background intensity of an empty glass cell was subtracted.

4. Kinetic and Stereochemical Model Study by ^{1}H NMR Monitoring

For assessment of pFA, dFA and SpCp cycloaddition kinetics with maleimide and subsequent *endo/exo* ratio determination, a model study was completed by combining each diene crosslinker – **bispFAPEG**, **bisdFAPEG**, or **bisSpCpPEG** – with a small molecule maleimide: 3-maleimideopropionic acid (**mal-COOH**). Solutions of each diene crosslinker were prepared in D2O at a concentration of 2.5 mM and spiked with ethylene carbonate as an internal standard for determination of reaction conversion. Initial ^{1}H NMR spectra were recorded (t = 0) before **mal-COOH** (2 eq from 250 mM stock solution) was added to each solution. ^{1}H NMR spectra were collected periodically to determine conversion. *Endo/exo* ratios were determined by relative integrations of resonances corresponding to each stereoisomer.

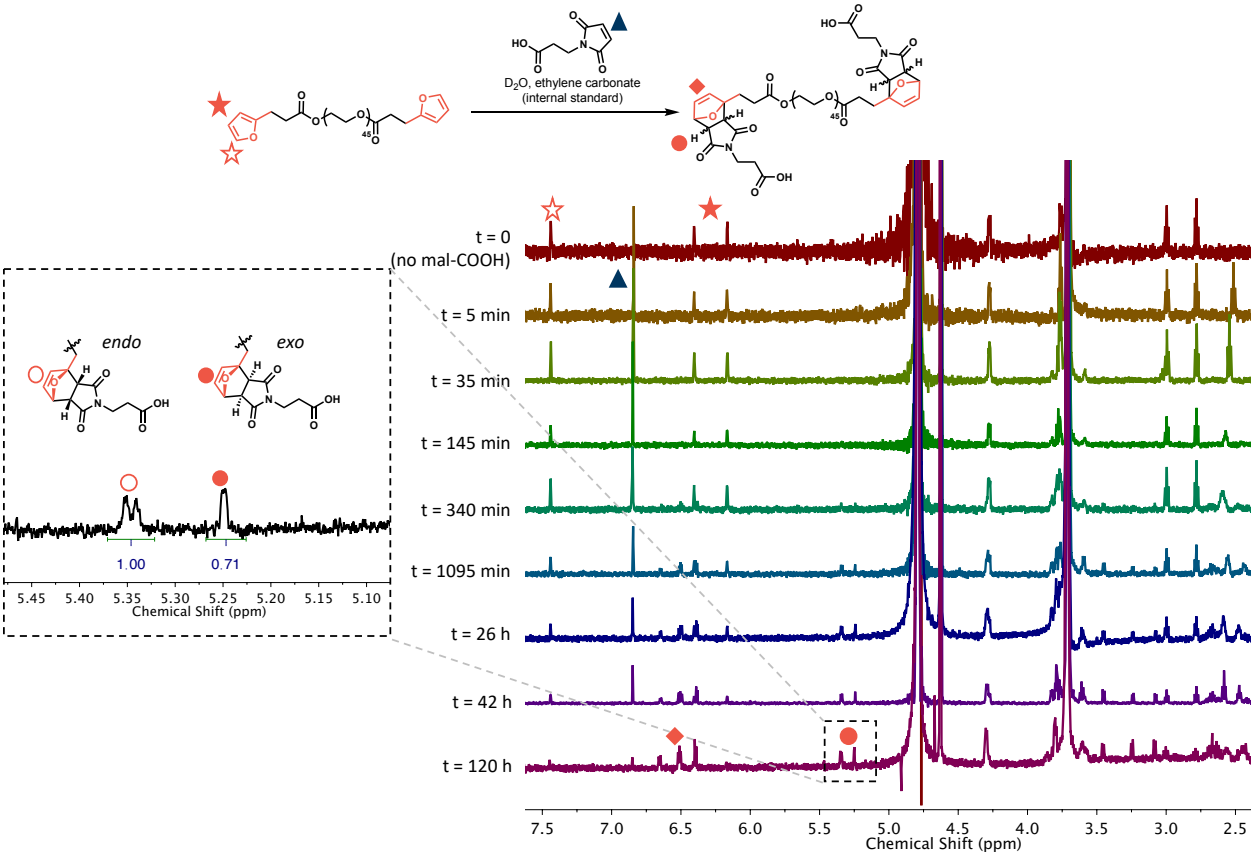

Figure S15. Monitoring of cycloaddition between **bispFAPEG** with **mal-COOH** over 120 h in D_2O. Near-complete disappearance of furan resonances (red stars) is observed after 120 h and appearance of diagnostic **pFA–mal** cycloadduct peaks are observed at 5.3 (red circle) and 6.4 ppm (red diamond). Integration of *endo* and *exo* resonances indicate a final *endo*:*exo* ratio of 1:0.7 is obtained.

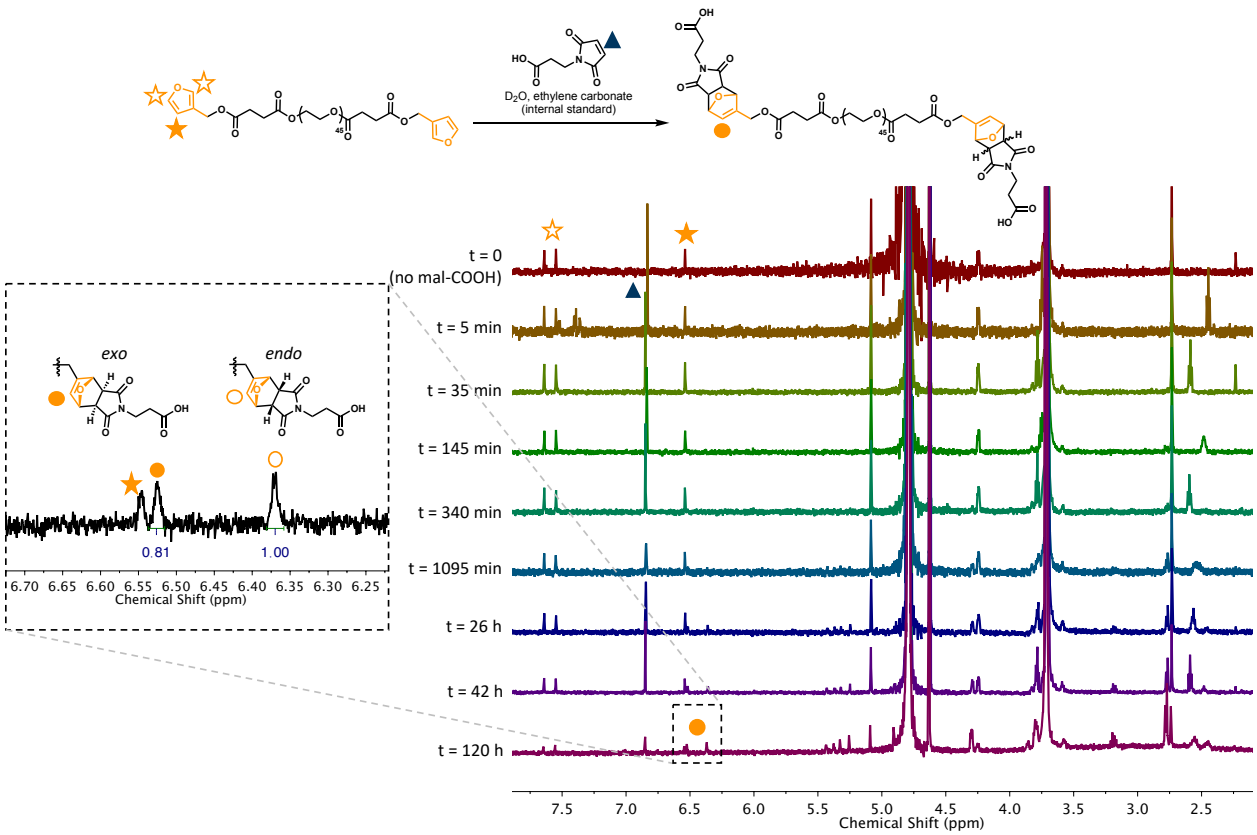

Figure S16. Monitoring of cycloaddition between **bisdFAPEG** with **mal-COOH** over 120 h in D_2O. Near-complete disappearance of furan resonances (orange stars) is observed after 120 h and appearance of diagnostic **dFA–mal** cycloadduct peaks are observed at 6.4 ppm (orange circle). Integration of *endo* and *exo* resonances indicate a final *endo*:*exo* ratio of 1:0.8 is obtained.

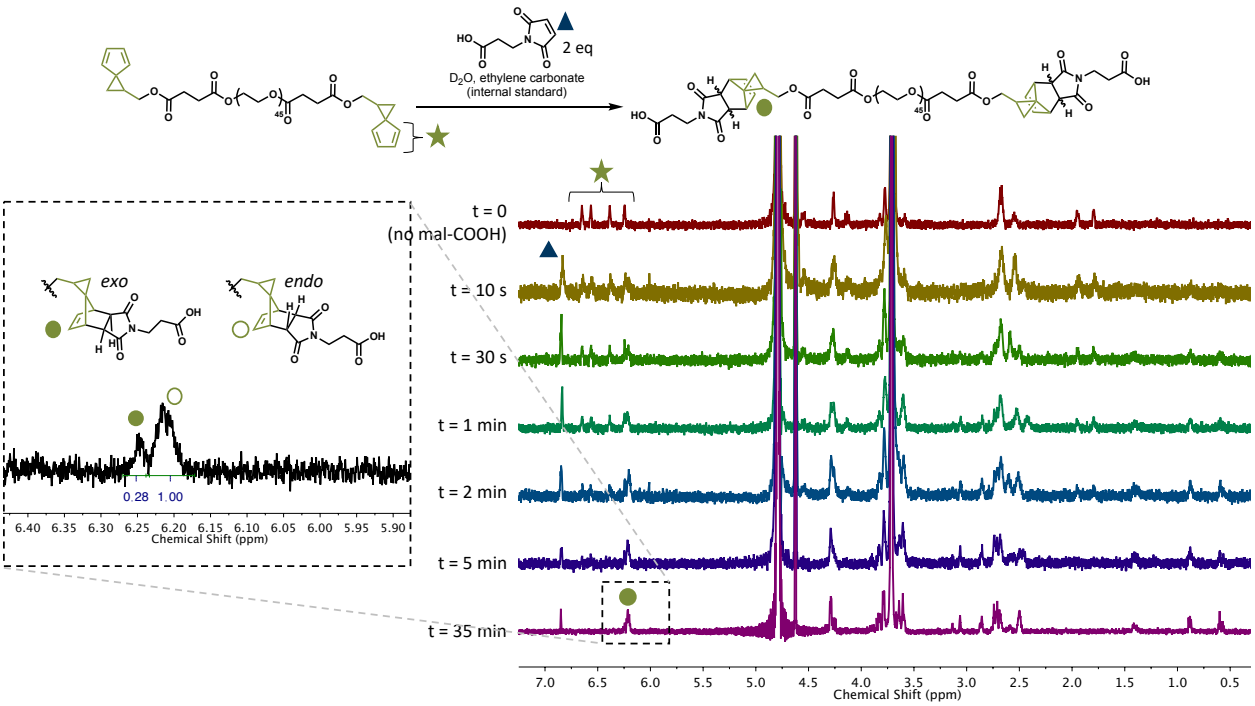

Figure S17. Monitoring of cycloaddition between **bisSpCpPEG** with **mal-COOH** over 35 min in D_2O. Complete disappearance of SpCp resonances (green stars) is observed after 35 min and appearance of diagnostic **SpCp–mal** cycloadduct peaks are observed at 6.2 ppm (green circle). Integration of *endo* and *exo* resonances indicate a final *endo*:*exo* ratio of 1:0.3 is obtained.

5. Constrained Geometries Simulate External Force Calculations

DFT calculations were performed following previously established methods[19,20] using Gaussian16 at the B3LYP/6-31+G(d,p) level of theory in the gas phase.[21] Starting from each ground state optimized geometry for each DA adduct a redundant coordinate scan was run while displacing the indicated atoms by 0.05 Å for 100 steps and/or until a bond was broken. The energy relative to the ground state equilibrium geometry (i) is plotted against the displacement to afford CoGEF curves which provide bond dissociation energy as the maximum energy before scission (E_{max}). Additionally, the slope of these curves ($\Delta E/\Delta\Delta D$) provides a measure of the force imparted on the system. Maximum force (F_{max}) values are reported as the slope between the two points before bond scission (ii). CoGEF curves for each adduct are provided with the structures corresponding to the initial optimized geometry and the computed structure immediately after bond scission are provided below.

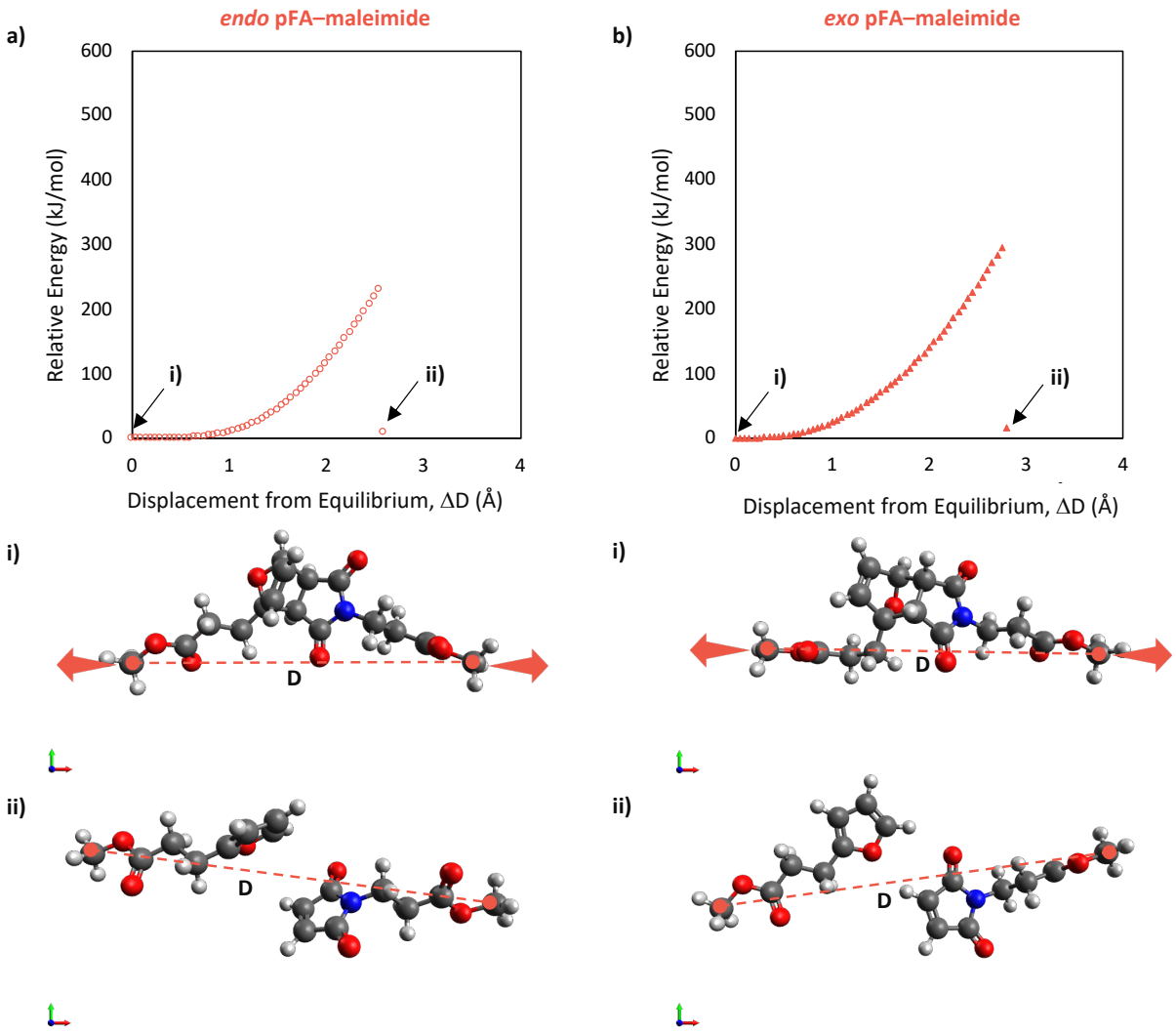

Figure S18. CoGEF results for pFA–maleimide adducts. a) Plot of relative energies versus displacement starting from optimized equilibrium geometry (i) of *endo* stereoisomer upon stepwise elongation. Computed structure upon scission (ii) indicates selective cycloreversion of the DA bond. b) Plot of relative energies versus displacement starting from optimized equilibrium geometry (i) of *exo* stereoisomer upon stepwise elongation. Computed structure upon bond scission (ii) indicates selective cycloreversion of the DA bond.

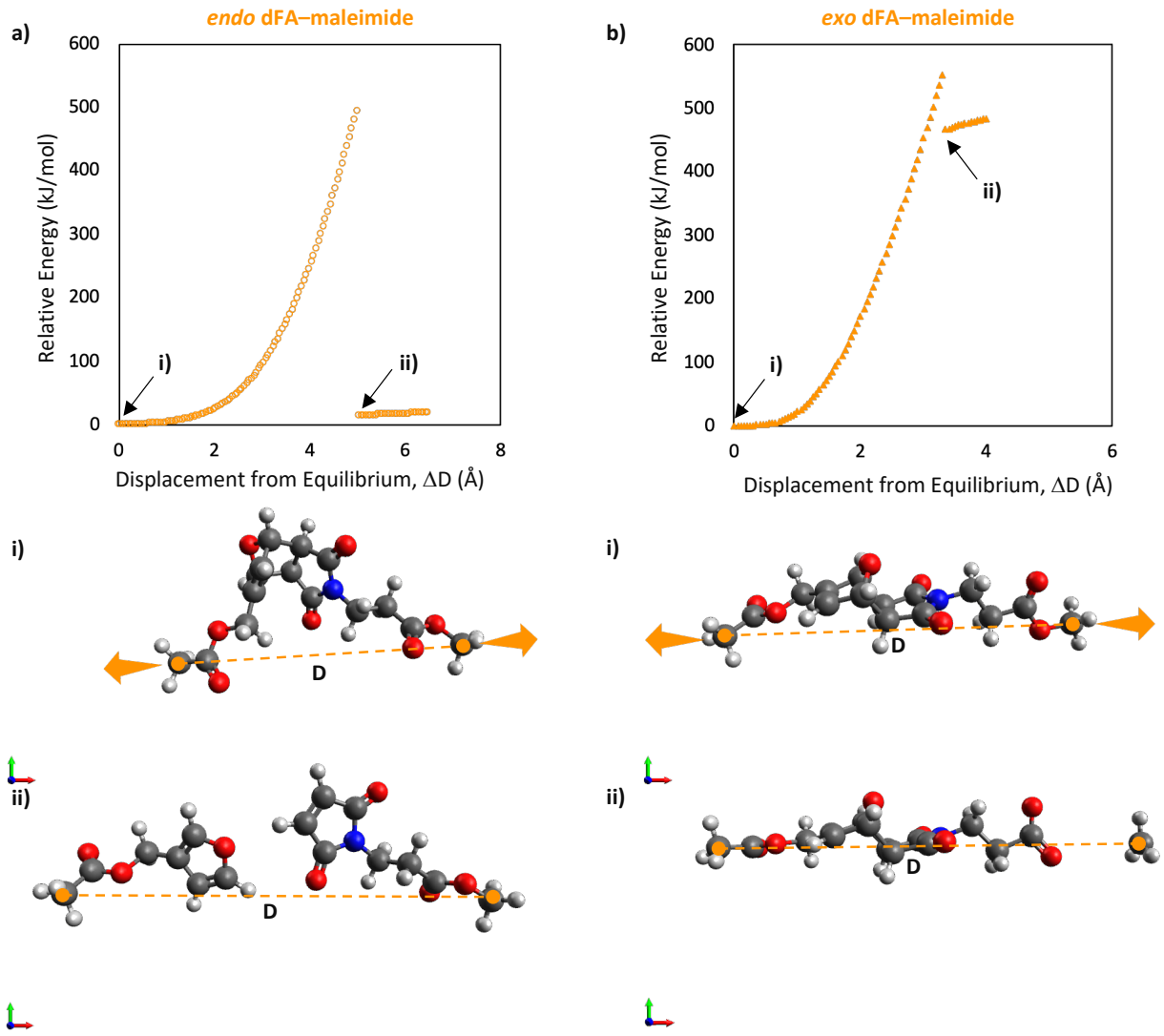

Figure S19. CoGEF results for dFA–maleimide adducts. a) Plot of relative energies versus displacement starting from optimized equilibrium geometry (i) of *endo* stereoisomer upon stepwise elongation. Computed structure upon scission (ii) indicates selective cycloreversion of the DA bond. b) Plot of relative energies versus displacement starting from optimized equilibrium geometry (i) of *exo* stereoisomer upon stepwise elongation. Computed structure upon bond scission (ii) indicates rupture of terminal non-DA bond.

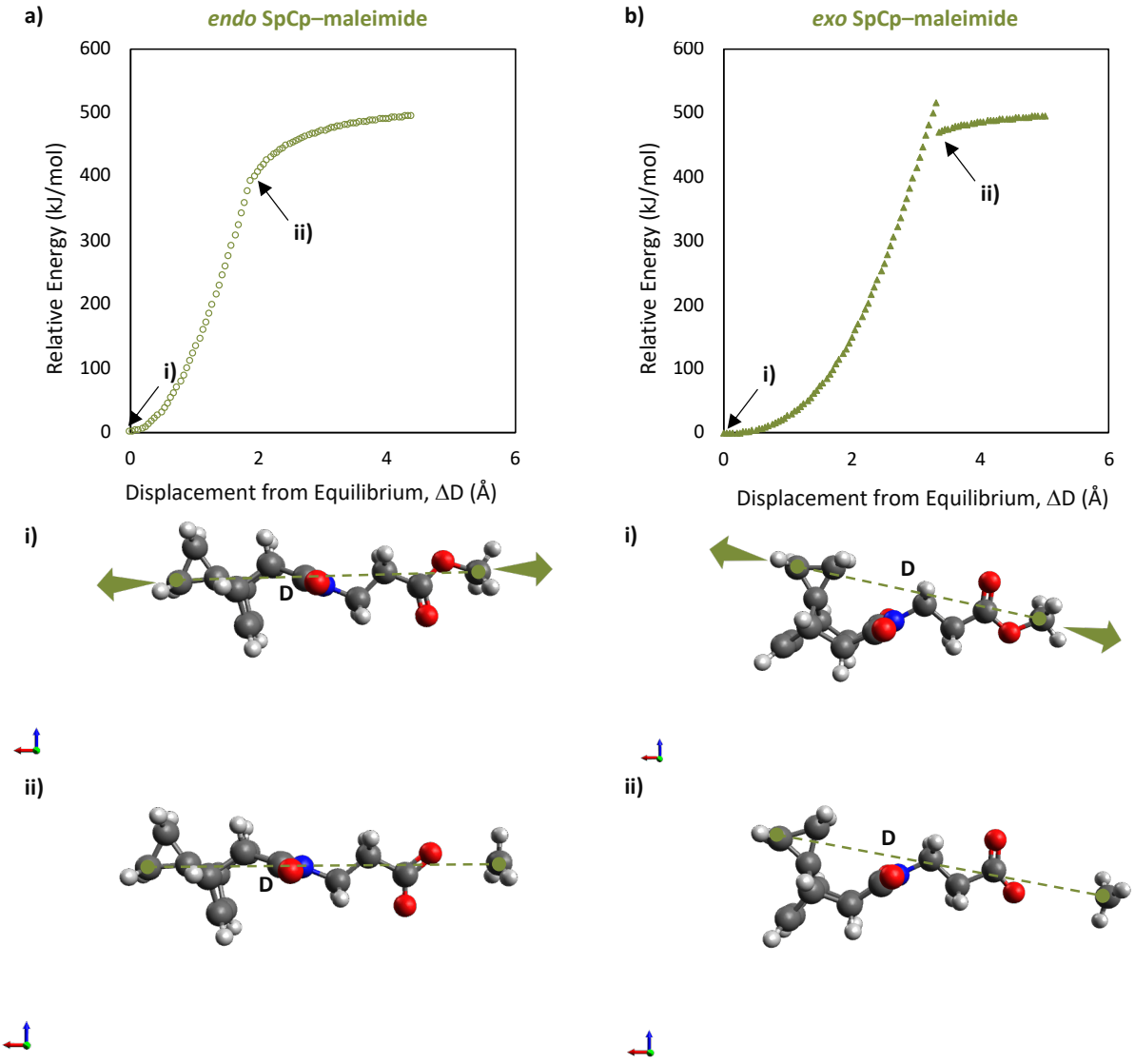

Figure S20. CoGEF results for SpCp–maleimide adducts. a) Plot of relative energies versus displacement starting from optimized equilibrium geometry (i) of *endo* stereoisomer upon stepwise elongation. Computed structure upon scission (ii) indicates rupture of terminal non-DA bond. b) Plot of relative energies versus displacement starting from optimized equilibrium geometry (i) of *exo* stereoisomer upon stepwise elongation. Computed structure upon bond scission (ii) indicates rupture of terminal non-DA bond.

The cartesian coordinates for the optimized ground state geometries and post-scission geometries are listed below.

***endo* pFA–maleimide equilibrium geometry (i)**

C	0.67830500	-0.39357500	-0.38580000
C	-0.41511100	0.47399200	-0.98507800
C	0.14109900	1.91117600	-0.93928700
C	1.52608300	1.78449400	-0.32874500
N	1.75413300	0.43391400	-0.04975100
O	2.32253700	2.67691800	-0.10251200
O	0.65810200	-1.59785200	-0.20843100

C	2.96584900	-0.05534800	0.60537500
H	2.68512000	-0.90989700	1.22312500
H	3.33607300	0.74214200	1.25156200
C	-1.75396600	0.61472200	-0.14024900
C	-1.33667600	0.85358900	1.31243900
C	-0.85118800	2.09943200	1.36096700
C	-0.95931500	2.63123900	-0.06064000
O	-2.13013400	1.95495900	-0.54619700
H	-1.34706200	0.10318700	2.09414100
H	-0.37541800	2.61041300	2.18907300
C	-2.83291700	-0.40275000	-0.44871600
H	-2.45039100	-1.39775100	-0.19500900
H	-3.01623100	-0.40912400	-1.52772700
H	-1.03552800	3.70703700	-0.20507500
C	4.03414700	-0.45920400	-0.41583100
H	4.30456100	0.39141100	-1.05170200
H	3.65788000	-1.24489400	-1.08072700
C	-5.24439600	-1.09349700	-0.09881200
O	-5.20046300	-1.88452500	-1.01950100
C	7.46691600	-1.82109600	-0.12160300
H	7.94661400	-1.06419100	0.50322100
H	7.29083600	-2.72071500	0.47260600
H	8.08028000	-2.04781500	-0.99287200
H	-0.66088300	0.12073500	-1.98967700
H	0.20658000	2.39795600	-1.91491700
C	5.29050400	-0.96791200	0.25921700
O	6.22269400	-1.31878000	-0.65123300
O	5.45566000	-1.05584500	1.45941900
C	-7.44543700	-1.80542700	0.41467500
H	-8.19884000	-1.55702500	1.16155400
H	-7.81842600	-1.60369100	-0.59231600
H	-7.16050600	-2.85761800	0.48788700
C	-4.14504300	-0.12803600	0.29108300
H	-4.49998900	0.88639500	0.07329900
H	-4.01872000	-0.17140800	1.37847200
O	-6.31814600	-0.95779400	0.71212700

Electronic Energy: -1202.546165 Hartree

***endo* pFA–maleimide post-scission geometry (ii)**

C	2.05092000	-1.72249100	0.56242400
C	0.80967000	-2.13340400	-0.17680700
C	0.61236300	-1.27929000	-1.18701800
C	1.71469900	-0.25867800	-1.17398000
N	2.54085000	-0.58805500	-0.09400200
O	1.88249500	0.67556500	-1.93541200
O	2.55469200	-2.24859900	1.53661500
C	3.73139100	0.15457800	0.30384600
H	3.79393900	0.12705500	1.39345100
H	3.59146100	1.19133400	-0.00646900
C	-2.92979400	0.80798000	0.61537200
C	-2.20817600	1.47549700	1.56354200

C	-1.15750000	2.17258500	0.87346000
C	-1.31242800	1.88183600	-0.44723400
O	-2.38722800	1.04993700	-0.62343000
H	-2.39932600	1.46966100	2.62748100
H	-0.39345100	2.80333100	1.30526600
C	-4.13536400	-0.07009300	0.66458300
H	-4.35668400	-0.29200200	1.71245900
H	-3.92470100	-1.03223700	0.18347800
H	-0.77602600	2.15885600	-1.34137400
C	5.00434200	-0.42892000	-0.32019600
H	4.94600800	-0.40305400	-1.41466500
H	5.12764500	-1.48011500	-0.03678600
C	-6.58480900	-0.33029000	0.03623200
O	-6.61762700	-1.46213400	0.47606200
C	8.60631900	0.40507200	-0.05674600
H	8.61678700	1.43705700	-0.41489100
H	8.74861800	0.39720500	1.02627200
H	9.37722500	-0.18385200	-0.55222700
H	0.21824200	-2.98704200	0.12693200
H	-0.18172500	-1.25395300	-1.92125300
C	6.24305100	0.32944200	0.10839900
O	7.35865000	-0.23299500	-0.40214000
O	6.25118900	1.31543900	0.81815300
C	-8.88806600	-0.46585000	-0.51336300
H	-9.63353400	0.20074100	-0.94582000
H	-8.77037100	-1.36233600	-1.12703000
H	-9.17239400	-0.75916400	0.49987000
C	-5.36576800	0.56796600	-0.00278200
H	-5.15711200	0.80979000	-1.05141200
H	-5.62372000	1.51860200	0.47807900
O	-7.66241300	0.29289700	-0.49256400

Electronic Energy: -1202.542218 Hartree

***exo* pFA–maleimide equilibrium geometry (i)**

C	0.71507300	-0.33722900	0.71959500
C	-0.44484100	0.58428600	1.07643100
C	-0.03876200	1.96160200	0.49452900
C	1.29106600	1.72061300	-0.20442800
N	1.64197200	0.38303600	-0.03406100
O	1.95583300	2.53687800	-0.81513100
O	0.84933400	-1.50757700	1.02799700
C	2.84827200	-0.21187700	-0.60628600
H	2.62487700	-1.25487200	-0.83545800
H	3.06432000	0.31570900	-1.53660500
C	-1.78455100	0.28667500	0.26776500
C	-2.79678800	1.29822200	0.81674800
C	-2.44668200	2.48682900	0.31405000
C	-1.20553900	2.22138500	-0.52532900
O	-1.44070500	0.88763600	-1.00448200
H	-3.57203200	1.05408200	1.53149900
H	-2.86428800	3.46370400	0.52651400

C	-2.19965300	-1.16651500	0.11223400
H	-2.37662400	-1.58726900	1.10703000
H	-1.36135600	-1.71961000	-0.31803700
C	-4.76159600	-1.18952600	-0.05802400
O	-4.91677600	-1.07062100	1.14272600
H	-0.61127000	0.55279500	2.15502800
H	0.07076800	2.77094000	1.21970500
C	-3.43711100	-1.37577300	-0.77105100
H	-3.44236800	-2.40219200	-1.15916900
H	-3.41378400	-0.72485000	-1.65041800
C	-7.10882700	-1.08687500	-0.37170700
H	-7.79009400	-1.13377800	-1.22063600
H	-7.30136600	-1.90640400	0.32469600
H	-7.21382300	-0.13524000	0.15469300
O	-5.78763600	-1.20563300	-0.93536300
C	4.03581500	-0.11559300	0.35697000
H	4.25297900	0.93011000	0.60240600
H	3.80993100	-0.62320600	1.30163200
O	5.36299600	-1.26416100	-1.32053100
C	5.28589300	-0.73706900	-0.22901100
C	7.57456100	-1.19553600	0.17253500
H	8.28087500	-1.01936200	0.98303500
H	7.46279600	-2.26546300	-0.01780200
H	7.90435100	-0.69905200	-0.74300600
O	6.32581200	-0.63374000	0.62565000
H	-0.96653700	2.89873100	-1.34374500

Electronic Energy: -1202.548898 Hartree

***exo* pFA–maleimide post-scission geometry (ii)**

C	-2.49743900	-2.35054900	0.17681000
C	-1.03258600	-2.32651500	-0.15246400
C	-0.60339600	-1.05979100	-0.11078700
C	-1.76607300	-0.17875000	0.25112500
N	-2.86826300	-1.02013600	0.40917000
O	-1.77760600	1.03141800	0.38744700
O	-3.23812900	-3.30972200	0.23830900
C	-4.20810800	-0.57964400	0.78098600
H	-4.68281500	-1.39534300	1.32913400
H	-4.10494000	0.27292000	1.45478800
C	3.34427400	1.42838300	0.09328800
C	3.55982000	2.77630900	0.05630700
C	2.27055000	3.40633700	0.16026200
C	1.35850900	2.40221100	0.25397100
O	1.99767000	1.18757400	0.21239900
H	4.51666200	3.27061400	-0.03250400
H	2.05857500	4.46599600	0.16529800
C	4.21563000	0.21667400	0.03106400
H	3.92323700	-0.40784700	-0.82223400
H	4.05032600	-0.40375700	0.92051300
C	6.57844500	-0.66724800	-0.16085300
O	6.19008900	-1.81228900	-0.16696000
H	-0.48289300	-3.23130500	-0.37632300

H	0.38608500	-0.65355500	-0.27738700
C	5.70035200	0.56405700	-0.08052100
H	6.03457300	1.16265700	0.77516900
H	5.89903200	1.17459000	-0.96978900
C	8.81833400	-1.41977800	-0.31566900
H	9.80267800	-0.95524100	-0.36325300
H	8.73561100	-2.06098200	0.56500400
H	8.62751000	-2.01411700	-1.21230700
O	7.88310900	-0.32589700	-0.22985100
C	-5.04210900	-0.19662500	-0.44634800
H	-4.54912900	0.59873700	-1.01679000
H	-5.14832200	-1.05059300	-1.12518100
O	-6.85705300	0.35706200	1.08677500
C	-6.42645100	0.28177900	-0.06083600
C	-8.48331700	1.09687400	-0.91143200
H	-8.89391800	1.31941600	-1.89560900
H	-9.07375600	0.32577200	-0.41114200
H	-8.46142200	1.99454100	-0.28916900
O	-7.14325800	0.62299400	-1.15525000
H	0.28354800	2.35699000	0.34521600

Electronic Energy: -1202.543109 Hartree

***endo* dFA–maleimide equilibrium geometry (i)**

C	-0.18937100	0.34516700	1.10251100
C	0.75028100	1.52269700	1.29922900
C	0.29373800	2.57760200	0.26870800
C	-0.88617600	1.94813600	-0.45055200
N	-1.09709900	0.67650900	0.09325100
O	-1.55289200	2.43023800	-1.34696400
O	-0.17895100	-0.71884000	1.69470000
C	-2.12490700	-0.24221300	-0.39512300
H	-1.74224700	-1.25766100	-0.28066700
H	-2.27274200	-0.03754500	-1.45657300
C	2.26048100	1.31456100	0.87480500
C	2.28810100	0.58698600	-0.47098200
C	1.88568800	1.50223900	-1.36482500
C	1.61944300	2.77058800	-0.57006600
O	2.58783900	2.66124800	0.49185900
H	1.70166400	1.37301800	-2.42488100
H	1.70610100	3.72459900	-1.08583200
C	-3.43983500	-0.07366300	0.37285500
H	-3.81347800	0.95253800	0.28039500
H	-3.29290800	-0.26275000	1.44212900
C	-6.75002900	-1.72434200	0.16359400
H	-7.02339400	-1.52593800	-0.87528300
H	-6.47379200	-2.77589700	0.26956700
H	-7.57048300	-1.47105500	0.83395400
H	0.70598300	1.86332200	2.33612500
H	-0.00401100	3.53261600	0.70714700
C	-4.51006400	-1.01619200	-0.13687200

O	-5.65421000	-0.87563000	0.56426700
O	-4.37439400	-1.79993200	-1.05467500
H	2.92208500	0.95281500	1.65820900
C	2.58721400	-0.85946600	-0.66645500
H	1.84772600	-1.50059900	-0.17332000
H	2.61231900	-1.12178000	-1.72720600
O	3.88464400	-1.12424300	-0.07114200
O	3.73192200	-3.26483800	-0.78296400
C	4.34251200	-2.39606500	-0.19649000
C	5.67683200	-2.56385300	0.48583300
H	6.07257300	-3.55502600	0.26562600
H	6.37637400	-1.79235800	0.15241100
H	5.55280200	-2.45097800	1.56777500

Electronic Energy: -1163.229085 Hartree

***endo* dFA–maleimide post-scission geometry (ii)**

C	-3.04876900	-2.13567000	-0.08908100
C	-1.67405900	-2.55487700	0.34392700
C	-0.90759000	-1.46339100	0.44917100
C	-1.73826700	-0.26206100	0.09278800
N	-3.01852900	-0.74098800	-0.20553300
O	-1.38591600	0.90293900	0.05819900
O	-4.01616600	-2.84015400	-0.30838300
C	-4.13861400	0.06851300	-0.67778800
H	-4.55913900	-0.41069800	-1.56512000
H	-3.73194400	1.03663900	-0.97424300
C	3.68241600	-0.95620500	0.43742900
C	4.47707400	-0.05041900	-0.20233000
C	3.64179900	1.10028300	-0.44081500
C	2.41615200	0.80294300	0.06776100
O	2.42387600	-0.45760900	0.60868100
H	3.92776200	2.02257900	-0.92647300
H	1.47321200	1.32652900	0.11876400
C	-5.22186300	0.23139900	0.39494600
H	-4.82964900	0.76578900	1.26847400
H	-5.56220700	-0.74681700	0.75015300
C	-8.61827500	1.71965000	0.39029800
H	-8.40098300	2.76515000	0.15977500
H	-9.05700400	1.24003400	-0.48764800
H	-9.28707800	1.64365900	1.24677600
H	-1.42157600	-3.59270400	0.51735300
H	0.13580200	-1.37243500	0.72367800
C	-6.42297600	0.99047000	-0.13074100
O	-7.41269000	1.03151600	0.78609900
O	-6.50399100	1.49938200	-1.23088800
H	3.85474400	-1.95408700	0.81130800
C	5.89743300	-0.25797900	-0.60710600
H	6.20414200	-1.29777500	-0.46556400
H	6.06169500	-0.00261100	-1.65825500
O	6.75474300	0.59558000	0.20394700
O	8.54676300	-0.23755800	-0.89619500

C	8.08230600	0.50135500	-0.05123200
C	8.88251000	1.41465800	0.84522500
H	8.73794800	1.12896100	1.89179700
H	9.93790900	1.34267000	0.58373800
H	8.53744400	2.44726100	0.73783300

Electronic Energy: -1163.224005 Hartree

***exo* dFA–maleimide equilibrium geometry (i)**

C	0.80475500	0.79856900	0.41782300
C	-0.57994800	0.38094100	-0.06016400
C	-0.39330600	-1.05304600	-0.61400600
C	1.08500900	-1.35898200	-0.41382100
N	1.68968200	-0.25210400	0.18236000
O	1.66524400	-2.38661200	-0.70900600
O	1.11104400	1.85995500	0.92770800
C	3.09595800	-0.22220800	0.58183300
H	3.16985300	0.39195900	1.48063100
H	3.38886300	-1.24407000	0.82749900
C	-1.56195900	0.11350100	1.14011000
C	-2.91356700	-0.25302800	0.52085300
C	-2.75087100	-1.49240700	0.03959000
C	-1.31318300	-1.87255600	0.36564200
O	-1.08517800	-1.16005600	1.59789300
H	-3.44777700	-2.08231300	-0.54099800
H	-0.96505200	1.12151600	-0.76464200
H	-0.66306800	-1.20063600	-1.66156700
C	3.98481200	0.34175800	-0.53122800
H	3.89668600	-0.26186700	-1.44170300
H	3.67725500	1.36007900	-0.79477900
O	5.88008500	0.00811400	0.94883700
C	5.44245300	0.37611000	-0.12256600
C	7.62532500	0.95628100	-0.83519600
H	8.07237600	1.37581200	-1.73570800
H	7.80658900	1.60464500	0.02514900
H	8.02942100	-0.03754700	-0.62919700
O	6.21213400	0.87518700	-1.11288200
H	-1.06234100	-2.92683700	0.46979600
H	-1.53685100	0.85572400	1.93761500
C	-4.06014700	0.69265400	0.44705900
H	-3.76044800	1.65233500	0.00610500
H	-4.45460000	0.91767300	1.44591800
O	-5.10281700	0.10441000	-0.35330400
O	-6.35540000	1.95741100	-0.02292000
C	-6.22618200	0.85340700	-0.50781200
C	-7.25233400	0.12921100	-1.34115800
H	-6.82622300	-0.14712500	-2.31012400
H	-7.55395800	-0.79537800	-0.83913300
H	-8.12029800	0.77225900	-1.48373600

Electronic Energy: -1163.232665 Hartree

***exo* dFA–maleimide post-scission geometry (ii)**

C	-0.68131200	-1.00431900	-0.04869900
C	0.67994400	-0.44671100	-0.47612100
C	0.44023900	1.07041400	-0.65937000
C	-1.03766200	1.27818800	-0.33184600
N	-1.61266000	0.04234000	-0.01967600
O	-1.63536600	2.33713300	-0.32534900
O	-0.93016700	-2.16038600	0.23127100
C	-2.98186600	-0.09574200	0.51295300
H	-2.99798300	-1.01328700	1.10145700
H	-3.16308100	0.75238300	1.17448300
C	1.72231500	-0.44838300	0.70734600
C	3.06095500	0.11533300	0.18639500
C	2.83083000	1.42484000	0.01929100
C	1.38575000	1.65562900	0.45396800
O	1.22598500	0.65575700	1.48210600
H	3.50455400	2.18169000	-0.36149700
H	1.03445300	-0.98608500	-1.35746400
H	0.65838400	1.47432800	-1.65008100
C	-4.05459000	-0.13854100	-0.58679300
H	-4.05269000	0.77109900	-1.19233600
H	-3.93928500	-1.00317600	-1.24469100
O	-5.61724200	-0.18219600	1.26787300
C	-5.56069900	-0.23596200	0.03368000
C	-10.38186800	-0.49817500	-0.34595900
H	-10.35018800	-1.45783300	-0.84658100
H	-10.35137800	-0.45009400	0.73555800
H	-10.42767500	0.41404300	-0.92761000
O	-6.41554900	-0.34234700	-0.87785100
H	1.11295100	2.64344200	0.82202900
H	1.74856500	-1.36391100	1.29822000
C	4.28013500	-0.72804100	-0.02802800
H	4.17733400	-1.37361800	-0.90967100
H	4.43487400	-1.39405500	0.82861200
O	5.46217000	0.09842100	-0.18939400
O	6.68824000	-1.80032600	-0.26671100
C	6.63999500	-0.58801800	-0.26917400
C	7.85916700	0.31622500	-0.32491100
H	7.67302200	1.19784300	-0.94282200
H	8.09239500	0.65881000	0.68897000
H	8.70179400	-0.25682400	-0.71078400

Electronic Energy: -1163.055075 Hartree

***endo* SpCp–maleimide equilibrium geometry (i)**

C	-0.27582100	-1.16973800	-0.20203700
C	-1.64767600	-0.77522300	-0.72151000
C	-1.64775900	0.77579600	-0.72102700
C	-0.27595500	1.17014100	-0.20127400
N	0.44255700	0.00015400	0.06187700
O	0.16133900	2.29398400	-0.03152200

O	0.16162400	-2.29363600	-0.03302300
C	1.79124600	0.00003700	0.62378500
H	1.88743500	-0.88797500	1.25052500
H	1.88759800	0.88820200	1.25028800
C	-2.87145900	-1.13454100	0.21048900
C	-2.52246700	-0.67216300	1.61898500
C	-2.52252500	0.67119400	1.61939700
C	-2.87158400	1.13440700	0.21118800
H	-2.23564800	-1.33004700	2.43180800
H	-2.23577600	1.32861000	2.43262200
H	-3.22274500	2.16132300	0.10262200
C	2.85875000	-0.00024400	-0.47526800
H	2.75140000	0.87948600	-1.11994800
H	2.75118900	-0.88028800	-1.11951300
C	6.56300500	0.00066700	-0.45015700
H	6.77417200	0.89080200	0.14700800
H	6.77446500	-0.89083400	0.14486500
H	7.15254000	0.00186600	-1.36631700
H	-1.79358500	-1.21302800	-1.71312000
H	-1.79369400	1.21420300	-1.71236800
C	4.25918800	-0.00040900	0.09960900
O	5.18697500	0.00096100	-0.88163700
O	4.53374700	-0.00168800	1.28279100
H	-3.22251900	-2.16142400	0.10128700
C	-3.81949000	0.00001100	-0.21330400
C	-4.68573000	0.00024800	-1.43819400
C	-5.30468400	-0.00007800	-0.04439100
H	-4.75713900	-0.91279200	-2.02483100
H	-4.75733400	0.91341100	-2.02459800
H	-5.78492600	0.91259900	0.29810000
H	-5.78505200	-0.91279000	0.29781500

Electronic Energy: -937.5138132 Hartree

***endo* SpCp–maleimide post-scission geometry (ii)**

C	-0.39793900	-1.16558700	-0.23393700
C	-1.82067400	-0.77114600	-0.68496700
C	-1.82068800	0.77118500	-0.68492400
C	-0.39795100	1.16563300	-0.23389600
N	0.40000300	0.00003200	-0.13595900
O	0.01417100	2.29066200	-0.02884500
O	0.01420200	-2.29060900	-0.02890300
C	1.80414300	0.00001800	0.41861300
H	1.87140500	-0.88636500	1.05036300
H	1.87142800	0.88638800	1.05038100
C	-3.07775100	-1.13393000	0.22957000
C	-2.73384900	-0.67167500	1.63780500
C	-2.73386200	0.67153600	1.63785400
C	-3.07777600	1.13388800	0.22965000
H	-2.44566000	-1.33035200	2.44947800
H	-2.44568900	1.33015800	2.44957600
H	-3.41257300	2.16641900	0.12016100

C	3.00845500	0.00001500	-0.59268600
H	2.98644000	0.88417300	-1.23571800
H	2.98643000	-0.88414000	-1.23572400
C	8.20301900	-0.00002900	-0.34818100
H	8.24556100	0.93276700	0.20020500
H	8.24558100	-0.94085300	0.18629900
H	8.19603100	0.00797200	-1.43049500
H	-1.96803800	-1.19911200	-1.68224900
H	-1.96807400	1.19920500	-1.68218100
C	4.47228400	0.00000000	0.14648400
O	5.46009800	0.00001900	-0.69686100
O	4.47992500	-0.00001400	1.37260400
H	-3.41254100	-2.16645600	0.12001000
C	-4.06404800	-0.00000800	-0.19604100
C	-4.93402400	0.00003100	-1.41844400
C	-5.61852400	-0.00001900	-0.05637000
H	-4.99286600	-0.91041800	-2.01215500
H	-4.99286900	0.91051700	-2.01209900
H	-6.08832900	0.91751700	0.28439100
H	-6.08831500	-0.91758900	0.28432100

Electronic Energy: -937.361956 Hartree

***exo* SpCp–maleimide equilibrium geometry (i)**

C	-0.40672900	-0.47067500	-1.16019000
C	-1.73455300	-1.10166600	-0.76472700
C	-1.73534900	-1.08491800	0.78850700
C	-0.40790400	-0.44561700	1.17168400
N	0.29932600	-0.15549800	0.00283000
O	0.00171100	-0.21273000	2.29457900
O	0.00406700	-0.26192100	-2.28740500
C	1.59789700	0.51380000	-0.00374000
H	1.64334600	1.13820400	-0.89756800
H	1.64403100	1.15384600	0.87890300
C	-2.99402000	-0.22717500	-1.13107000
C	-4.19411600	-1.04506500	-0.66145200
C	-4.19480800	-1.03059100	0.68142200
C	-2.99520500	-0.20271500	1.13455400
H	-4.85842400	-1.60016100	-1.31491500
H	-4.85979400	-1.57148700	1.34600700
H	-1.79432400	-2.09615000	-1.21429400
H	-1.79568800	-2.06945600	1.25937700
C	2.75116200	-0.49473900	0.00463700
H	2.69692600	-1.13825800	0.89009300
H	2.69622100	-1.15368600	-0.86934100
O	4.27587600	1.39480700	-0.01247400
C	4.09989100	0.19302600	-0.00189700
C	6.44105300	-0.16573500	0.00041900
H	7.10358100	-1.03051800	0.00778100
H	6.60241400	0.43778800	-0.89580800
H	6.60300600	0.45341000	0.88581900
O	5.10486500	-0.70853800	0.00562300

H	-3.00504200	0.17387100	2.15852400
H	-3.00276100	0.12722700	-2.16293800
C	-2.94266000	0.82131000	-0.00940800
C	-2.15120600	2.10004700	-0.02281700
C	-3.67220500	2.12668600	-0.02386200
H	-1.63895400	2.38292900	-0.93906800
H	-1.63980200	2.40267200	0.88758000
H	-4.17530300	2.44459300	0.88542200
H	-4.17435200	2.42488000	-0.94032400

Electronic Energy: -937.5149912 Hartree

***exo* SpCp–maleimide post-scission geometry (ii)**

C	-0.48850400	0.15871200	1.16652900
C	-1.71318300	0.98096500	0.77465300
C	-1.71328500	0.98007600	-0.77597300
C	-0.48842600	0.15773500	-1.16712000
N	0.22065500	-0.16571200	-0.00014400
O	-0.12839300	-0.13733800	-2.29095500
O	-0.12860000	-0.13555900	2.29061800
C	1.54384700	-0.80796300	0.00027900
H	1.61158900	-1.43432400	0.88992800
H	1.61181200	-1.43530500	-0.88865400
C	-3.14052400	0.42072400	1.13337200
C	-4.09593500	1.52354700	0.67053400
C	-4.09603100	1.52258300	-0.67238600
C	-3.14066300	0.41909400	-1.13374300
H	-4.59999500	2.22260900	1.32920800
H	-4.60018100	2.22070000	-1.33199200
H	-1.57302700	1.97131200	1.21873700
H	-1.57356500	1.96992800	-1.22128200
C	2.65102700	0.26165800	-0.00019900
H	2.59860000	0.89531200	-0.88913500
H	2.59825100	0.89655200	0.88780700
O	4.20583600	-1.59728200	-0.00105200
C	4.15561700	-0.36290200	0.00019300
C	9.02472500	0.73573600	0.00018000
H	8.80142700	1.76911100	0.23384300
H	9.15542600	0.01588100	0.79848100
H	9.10006200	0.41811500	-1.03225300
O	5.00968600	0.55666100	0.00157200
H	-3.24263000	0.06870100	-2.16201700
H	-3.24243400	0.07171300	2.16212100
C	-3.37993400	-0.59160500	0.00052800
C	-3.03316800	-2.05101800	0.00155700
C	-4.49440700	-1.60249600	0.00128300
H	-2.63697700	-2.48862000	0.91467400
H	-2.63690800	-2.48998200	-0.91087200
H	-5.06565000	-1.73694500	-0.91306500
H	-5.06554000	-1.73569800	0.91588400

Electronic Energy: -937.3355523 Hartree

6. References

(1) de Figueiredo, R.; Oczipka, P.; Fröhlich, R.; Christmann, M. Synthesis of 4-Maleimidobutyric Acid and Related Maleimides. *Synthesis* **2008**, *2008* (8), 1316–1318. https://doi.org/10.1055/s-2008-1032016.

(2) Kassianidis, E.; Pearson, R. J.; Philp, D. Probing Structural Effects on Replication Efficiency through Comparative Analyses of Families of Potential Self-Replicators. *Chem. - Eur. J.* **2006**, *12* (34), 8798–8812. https://doi.org/10.1002/chem.200600460.

(3) St. Amant, A. H.; Lemen, D.; Florinas, S.; Mao, S.; Fazenbaker, C.; Zhong, H.; Wu, H.; Gao, C.; Christie, R. J.; Read de Alaniz, J. Tuning the Diels–Alder Reaction for Bioconjugation to Maleimide Drug-Linkers. *Bioconjug. Chem.* **2018**, *29* (7), 2406–2414. https://doi.org/10.1021/acs.bioconjchem.8b00320.

(4) Shull, K. R.; Ahn, D.; Chen, W.-L.; Flanigan, C. M.; Crosby, A. J. Axisymmetric Adhesion Tests of Soft Materials. *Macromol. Chem. Phys.* **1998**, *199* (4), 489–511. https://doi.org/10.1002/(SICI)1521-3935(19980401)199:4<489::AID-MACP489>3.0.CO;2-A.

(5) Hu, Y.; Zhao, X.; Vlassak, J. J.; Suo, Z. Using Indentation to Characterize the Poroelasticity of Gels. *Appl. Phys. Lett.* **2010**, *96* (12), 2008–2011. https://doi.org/10.1063/1.3370354.

(6) Chan, E. P.; Hu, Y.; Johnson, P. M.; Suo, Z.; Stafford, C. M. Spherical Indentation Testing of Poroelastic Relaxations in Thin Hydrogel Layers. *Soft Matter* **2012**, *8* (5), 1492–1498. https://doi.org/10.1039/c1sm06514a.

(7) Fakhouri, S.; Hutchens, S. B.; Crosby, A. J. Puncture Mechanics of Soft Solids. *Soft Matter* **2015**, *11* (23), 4723–4730. https://doi.org/10.1039/c5sm00230c.

(8) Rattan, S.; Crosby, A. J. Effect of Far-Field Compliance on Local Failure Dynamics of Soft Solids. *Extreme Mech. Lett.* **2018**, *24*, 14–20. https://doi.org/10.1016/j.eml.2018.08.003.

(9) Rattan, S.; Li, L.; Lau, H. K.; Crosby, A. J.; Kiick, K. L. Micromechanical Characterization of Soft, Biopolymeric Hydrogels: Stiffness, Resilience, and Failure. *Soft Matter* **2018**, *14* (18), 3478–3489. https://doi.org/10.1039/c8sm00501j.

(10) Rattan, S.; Crosby, A. J. Effect of Polymer Volume Fraction on Fracture Initiation in Soft Gels at Small Length Scales. *ACS Macro Lett.* **2019**, *8*, 492–498. https://doi.org/10.1021/acsmacrolett.9b00086.

(11) Lake, G. J.; Thomas, A. G. The Strength of Highly Elastic Materials. *Proc. R. Soc. Lond. Ser. Math. Phys. Sci.* **1967**, *300* (1460), 108–119.

(12) Flory, P. J. Network Structure and the Elastic Properties of Vulcanized Rubber. *Chem. Rev.* **1944**, *35* (1), 51–75. https://doi.org/10.1021/cr60110a002.

(13) Stevenson, A.; Ab Malek, K. On The Puncture Mechanics of Rubber. *Rubber Chem. Technol.* **1994**, *67* (5), 743–760.

(14) Shergold, O. A.; Fleck, N. A. Experimental Investigation Into the Deep Penetration of Soft Solids by Sharp and Blunt Punches, With Application to the Piercing of Skin. https://doi.org/10.1115/1.1992528.

(15) Lin, W.; Otim, K. J.; Lenhart, J. L.; Cole, P. J.; Shull, K. R. Indentation Fracture of Silicone Gels. *J. Mater. Res.* **2009**, *24* (03), 957–965. https://doi.org/10.1557/jmr.2009.0128.

(16) Heller, W. T. Small-Angle Neutron Scattering and Contrast Variation: A Powerful Combination for Studying Biological Structures. *Acta Crystallogr. D Biol. Crystallogr.* **2010**, *66* (11), 1213–1217. https://doi.org/10.1107/S0907444910017658.

(17) Heller, W. T.; Urban, V. S.; Lynn, G. W.; Weiss, K. L.; O'Neill, H. M.; Pingali, S. V.; Qian, S.; Littrell, K. C.; Melnichenko, Y. B.; Buchanan, M. V.; Selby, D. L.; Wignall, G. D.; Butler, P. D.; Myles, D. A. The Bio-SANS Instrument at the High Flux Isotope Reactor of Oak Ridge National Laboratory. *J. Appl. Crystallogr.* **2014**, *47* (4), 1238–1246. https://doi.org/10.1107/S1600576714011285.

(18) Yao, X.; Avery, B.; Bobrek, M.; Debeer-Schmitt, L.; Geng, X.; Gregory, R.; Guyotte, G.; Harrington, M.; Hartman, S.; He, L.; Heroux, L.; Kasemir, K.; Knudson, R.; Kohl, J.; Lionberger, C.; Littrell, K.; Pearson, M.; Pingali, S. V.; Pratt, C.; Qian, S.; Ruiz-Rodriguez, M.; Sedov, V.; Taufer, G.; Urban, V.; Vodopivec, K. A Unified User-Friendly Instrument Control and Data Acquisition System for the ORNL SANS Instrument Suite. *Appl. Sci.* **2021**, *11* (3), 1216. https://doi.org/10.3390/app11031216.

(19) Klein, I. M.; Husic, C. C.; Kovács, D. P.; Choquette, N. J.; Robb, M. J. Validation of the CoGEF Method as a Predictive Tool for Polymer Mechanochemistry. *J. Am. Chem. Soc.* **2020**, *142* (38), 16364–16381. https://doi.org/10.1021/jacs.0c06868.

(20) Beyer, M. K. The Mechanical Strength of a Covalent Bond Calculated by Density Functional Theory. *J. Chem. Phys.* **2000**, *112* (17), 7307–7312. https://doi.org/10.1063/1.481330.

(21) Gaussian 16, Revision C.01, Frisch, M. J.; Trucks, G. W.; Schlegel, H. B.; Scuseria, G. E.; Robb, M. A.; Cheeseman, J. R.; Scalmani, G.; Barone, V.; Petersson, G. A.; Nakatsuji, H.; Li, X.; Caricato, M.; Marenich, A. V.; Bloino, J.; Janesko, B. G.; Gomperts, R.; Mennucci, B.; Hratchian, H. P.; Ortiz, J. V.; Izmaylov, A. F.; Sonnenberg, J. L.; Williams-Young, D.; Ding, F.; Lipparini, F.; Egidi, F.; Goings, J.; Peng, B.; Petrone, A.; Henderson, T.; Ranasinghe, D.; Zakrzewski, V. G.; Gao, J.; Rega, N.; Zheng, G.; Liang, W.; Hada, M.; Ehara, M.; Toyota, K.; Fukuda, R.; Hasegawa, J.; Ishida, M.; Nakajima, T.; Honda, Y.; Kitao, O.; Nakai, H.; Vreven, T.; Throssell, K.; Montgomery, J. A., Jr.; Peralta, J. E.; Ogliaro, F.; Bearpark, M. J.; Heyd, J. J.; Brothers, E. N.; Kudin, K. N.; Staroverov, V. N.; Keith, T. A.; Kobayashi, R.; Normand, J.; Raghavachari, K.; Rendell, A. P.; Burant, J. C.; Iyengar, S. S.; Tomasi, J.; Cossi, M.; Millam, J. M.; Klene, M.; Adamo, C.; Cammi, R.; Ochterski, J. W.; Martin, R. L.; Morokuma, K.; Farkas, O.; Foresman, J. B.; Fox, D. J. Gaussian, Inc., Wallingford CT, **2016**.